CONTRAST ENHANCED MRI AND ITS BIOLOGICAL APPLICATIONS

by

SUNBOK LEE

(Under the Direction of Qun Zhao)

ABSTRACT

Contrast enhanced MRI has many applications. Among those applications, positive contrast mapping and dynamic contrast enhance MRI (DCE-MRI) will be discussed in this thesis. Cells labeled with paramagnetic contrast agent can be detected by a negative contrast or signal loss in T_2 weighted image. In order to overcome the drawback of negative contrast method, recent research has focused on the positive contrast techniques such as white marker, inversion recovery on resonance water suppression (IRON), energy spectrum method, and susceptibility gradient mapping (SGM). In this thesis, newly developed positive contrast technique referred to as phase gradient mapping (PGM) will be discussed. The results of two positive contrast methods, SGM and PGM, are compared. In addition to these contrast enhanced MRI techniques, dynamic contrast enhanced technique (DCE-MRI) also is discussed and demonstrated using *in vivo* dog brain tumor data.

INDEX WORDS: Contrast enhanced MRI, dynamic contrast enhanced MRI, positive contrast, kinetics, tumor detection.

CONTRAST ENHANCED MRI AND ITS BIOLOGICAL APPLICATIONS

by

SUNBOK LEE

B.S., Sogang University, South Korea, 2002

A Thesis Submitted to the Graduate Faculty of The University of Georgia in Partial Fulfillment of the Requirements for the Degree

MASTER OF SCIENCE

ATHENS, GEORGIA

2008

CONTRAST ENHANCED MRI AND ITS BIOLOGICAL APPLICATIONS

by

SUNBOK LEE

Major Professor:	Qun Zhao
Committee:	Yiping Zhao Cheolwoo Park

Electronic Version Approved:

Maureen Grasso
Dean of the Graduate School
The University of Georgia
December 2008

ACKNOWLEDGEMENTS

I would like to thank my mother. Without her love and sacrifice, I couldn’t make anything. I also would like to thank my advisor Dr.Zhao, who gave me an opportunity to finish my master’s thesis and many invaluable lessons about research. Jason in our lab helped me a lot, thank you. Finally, I would like to thank all the KCC members.

TABLE OF CONTENTS

CHAPTER 1. INTRODUCTION

1.1 Motivation

Magnetic resonance imaging (MRI) is a non-invasive imaging technique primarily used in medical imaging. MRI originated from the nuclear magnetic resonance (NMR) which is also widely used in chemistry for spectroscopy. Cancer has been one of the main threats to human health for a long time. It is well known that cancer mortality can be reduced by an early detection. Also after the cancer treatment, the assessment of antiangiogenic treatment is essential. Magnetic resonance imaging (MRI) can be used to detect a tumor in the body without a surgery and also can be used to assess the effect of antiangiogenic treatment. Cells labeled with paramagnetic contrast agent can be detected by a negative contrast or dark signal loss in T_2 weighted image. However, some drawbacks of negative contrast method which will be discussed later motivate the research for positive contrast technique for paramagnetic contrast agent. In this thesis, several contrast enhanced MRI techniques were explained and demonstrated as positive contrast techniques. The contrast enhanced MRI techniques include White marker [1], IRON [2], SGM [3], energy spectrum method [4], and phase spatial gradient mapping. Among them, phase spatial gradient mapping (PGM) is newly developed method and has several advantages over the other positive contrast methods. It requires no pulse sequence manipulation and has no inherent uncertainty. SGM, energy spectrum method, and phase spatial gradient mapping were implemented using MATLAB (The Mathworks, MA.) and the results were compared.

Contrast enhanced MRI techniques can be considered as a static method in the sense that it only uses the image at a certain fixed time point. There has been effort to use time series of images to detect cancer. This method is called as a dynamic contrast enhanced MRI (DCE-MRI). DCE-MRI also were explained and demonstrated in this thesis.

1.2 MRI overview

All materials consist of atoms and all atoms have nuclei which are protons and neutrons as its component. Nuclei can possess angular momentum due to its spinning about an axis. This existence of angular momentum of particle itself is commonly referred to as nuclear spin. If nuclei have an odd number of protons, such as hydrogen atom (H), then it can have net spin. Proton is a spin half particle which means it can exist one of the two possible states in the presence of external magnetic field. If spin half particle such as proton is located in the external magnetic field, the spin can be parallel or anti parallel to the external magnetic field. The parallel spin has lower energy than the anti parallel spin. The ratio of protons in the two possible energy states can be determined by the equation derived from Boltzmann statistics [5]

$$\frac{N_{-}}{N_{+}} = e^{-\frac{\Delta E}{KT}} \tag{1.1}$$

where N_{-} and N_{+} are the number of proton which are lower energy state and higher energy state respectively. ΔE is the energy difference between the two possible states. T is the Kelvin temperature and K is the Boltzmann constant. Since proton has positive charge and also has spin, it can possess magnetic moment. Also in the presence of external magnetic field B_0, the magnetic moment precess with Larmor frequency $\omega = \gamma B_0$ and the precession axis is parallel to the external magnetic field B_0, say z direction. The summation of magnetic moment produced by

each spin in a given volume forms a net magnetic moment which is usually called magnetization vector $\vec{M}$. Basically, MRI manipulates this magnetization vector $\vec{M}$ using a RF pulse and reconstruct image using the signal from the movement of this $\vec{M}$. If there is only external magnetic field B_0 without any perturbation by RF pulse, then $\vec{M}$ is parallel along the direction of B_0 direction. This is called equilibrium state of magnetization and magnetization can be expressed by $\vec{M} = M_0\hat{z}$ when external magnetic field is also applied along z direction, i.e. $\vec{B} = B_0\hat{z}$.

The RF pulse produces an oscillating magnetic field in a plane perpendicular to the sample magnetization vector and this oscillating field plays a role to flip the net magnetization vector into the transverse plane which is perpendicular to the original net magnetic vector. After flipping into transverse plane, the magnetization vector will start to rotate around the z axis and can be detected by a coil placed perpendicular to its axis of rotation. Once the RF energy perturbation ceases, the transverse magnetization will decay to zero as the spin system returns to its equilibrium state, inducing an emf in the detection coil. This process is termed as free induction decay (FID). The time constant that describes how flipped $\vec{M}$ returns to its equilibrium value is called the spin lattice relaxation time (T_1). This process is related to the energy transfer between the spin system and lattice. The equation [5] governing this process is

$$M_Z = M_0(1-e^{t/T_1}) \qquad (1.2)$$

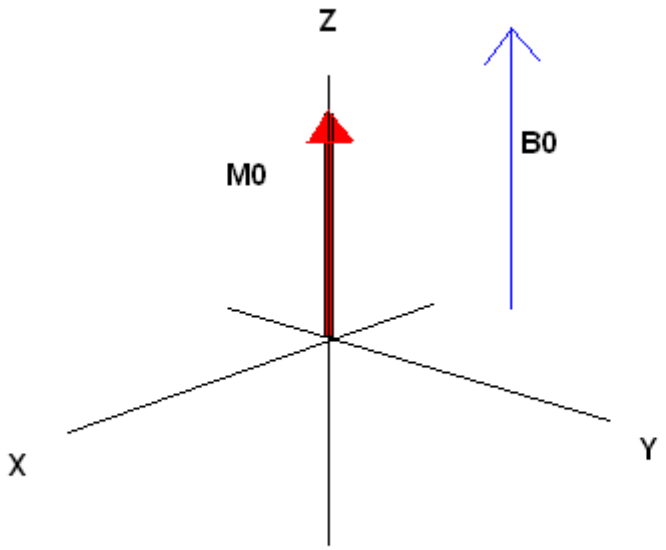

Figure 1.1 Magnetization vector ($\vec{M}$) is the sum of magnetic moment vector ($\vec{\mu}$) of all the spins in a given volume. When there is no perturbation by RF pulse sequence, it is said to be in its equilibrium state and $\vec{M}$ is parallel to the external magnetic field B_0 i.e. $\vec{M} = M_0\hat{z}$. $\vec{M}$ will flip into transverse plane (XY plane here) when RF pulse is applied. Once $\vec{M}$ flipped into transverse plane, it starts to rotate with Larmor frequency.

The spin-spin relaxation process also refers the loss of coherence of the transverse component of magnetization which is called dephasing of magnetization. T_2 relaxation time characterize this dephasing process. This dephasing process is governed by the following equation [5]

$$M_{XY} = M_0 e^{t/T_2} \tag{1.3}$$

The net magnetization in the XY plane, M_{XY}, goes to zero and then the longitudinal magnetization , M_Z, grows in until we have M_0 along Z. Both T_1 and T_2 are the characteristic of tissue and these two parameters are the basis of MRI contrast. Free induction decay (FID) signal which is mentioned above contains the information of these two parameters. In MRI, spatial information is further encoded into this FID using frequency encoding gradient and phase encoding gradient to locate or differentiate the signal from each voxel. The signal which we detect from the coil is the sum of all these FID from each voxel throughout the scanned object. This signal is used to reconstruct the image using Fourier transformation.

1.3 The effect of contrast agent on relaxation time.

A contrast agent is used to enhance the specific target of a subejct by changing a relaxation time. An increase in the T_1 relaxation rate will result in increasing the MR signal intensity, whereas an increase in the T_2 relaxation rate will tend to reduce the signal intensity. The enhancement of T_2 relaxation can be explained by susceptibility effect [6]. The suscepbility χ is defined as the proportional constant between the induced magnetization , M , of a substance and the applied magnetic field H [6]

$$M = \chi H \tag{1.4}$$

For values of $\mu_0 mH / kT << 1$, χ could be approximated as the following equation [6]

$$\chi = \frac{Nm^2\mu_0}{3kT} \tag{1.5}$$

,where N is the number of atoms per unit volume, m is the magnetic moment per atom, k is the Boltzmann's contant, μ_0 is the permeability of free space and T is the temperature in Kelvin. Therefore, for paramagnetic agents, the susceptibility is proportional to the concentration of paramagnetic atoms in tissue and the square of the magnetic moment of the agent. This magnetization differences , ΔM , within a given volume element in the image cause the increase in T_2 relaxation rates, which result in reduction in signal intensity. The compartmentalization of the contrast agent in tissue can also affect the T_1 relaxation rate by restricting water access to the contrast agent site. In a two-compartment water exchange limited spin system, the T_1 relaxation is described by a biexponential function [6]:

$$M(t) = M_0 = c_1 \exp(-u_1 t) + c_2 \exp(-u_2 t) \tag{1.6}$$

,where M_0 is the equilibrium magnetization and c_1, c_2 and u_1, u_2 are functions of the exchange rate, $1/\tau$.

1.4 Overview of this thesis

In this thesis, the techniques of contrast enhanced MRI, in which chemical substances called contrast agent is used to enhance contrast of image for specific purpose, and its biological applications are discussed. Among many techniques in contrast enhanced MRI, positive contrast mapping and dynamic contrast enhanced MRI (DCE-MRI) are discussed. In chapter 2, the previous methods for positive contrast mapping are reviewed and newly developed method referred to as phase gradient mapping (PGM) is presented. The results of SGM and PGM are compared using phantom and *in vivo* mouse data. In chapter 3, the principle of dynamic contrast

enhanced MRI (DCE-MRI) is reviewed and the physiological parameters estimated by DCE-MRI is used to differentiate various type of tumors.

CHAPTER 2.CONTRAST ENHANCED MRI

2.1 Contrast agent

Contrast agents are chemical substances which are used in anatomical or functional MRI to enhance the differences between different tissues by changing their relaxation rates. Contrast agent can affect the T_1 relaxation by preventing water to access near the contrast agent site, which is called water exchange effects. The effect of contrast agent on the T_2 relaxation can be termed as a susceptibility effect which refers to the increase in T_2 relaxation rates due to magnetic differences within a given voxel. An increase in the T_1 relaxation rate by a contrast agent causes an increase in the MR signal intensity but an increase in the T_2 relaxation rate make a reduction in the MR signal intensity [6].

Among many kind of contrast agents, contrast agents based on iron oxide were characterized by a large T_2 relaxation effect and slight T_1 relaxation so they produce dark signal loss in T_2 -weighted MR image. The iron oxides can be categorized by particle size.

Table 2.1 Classification of iron oxide contrast agent according to its size (From [6])

Name of iron oxide	Particle size
MION (Monocrystalline iron oxide nanopreparation)	Less than 20 nm
USPIO (Ultrasmall iron oxide particles)	Less than 50 nm
SPIO (Superparamagenetic iron oxide)	Greater than 50 nm

SPIO (SuperParamagenetic Iron Oxide) contrast agent was used as a liver specific contrast agent in mid 1980s [6]. Superparamagnetism refers to the generation of great magnetic moment of a particle in the presence of external magnetic field. Magnetic moment generated by superpamagnetism is the source of signal loss in T_2-weighted MR image and it disappears when the external magnetic field vanishes. SPIO contrast agent can be used in many MRI applications such as organ specific MRI [7], stem cell labeling and tracking [8], Passive tracking of interventional devices [9], MR angiography [10] and detection of tumor cell [3].

2.2 Motivation for positive contrast

Many application of SPIO contrast agent including researches mentioned above require technique for detecting and tracking SPIO contrast agent *in vivo*. Cells labeled by SPIO are usually detected by T_2- or T_2^*-weighted gradient echo image which shows dark signal loss at the site of SPIO. This signal loss can be explained as the following: Within a voxel, each spin rotates with its own Larmor frequency proportional to the magnetic field they are experiencing. Field inhomogeneity within voxel induced by SPIO makes each spin rotate with different frequency, which is called dephasing effect and this dephasing causes significant signal loss. Since signal void is used as an indication of presence of SPIO, this method is called negative contrast technique [11]. Whereas contrast agent such as gadolinium chelates is called a positive contrast agent since it brightens the local signal intensity by shortening T_1 relaxation time. The detection of SPIO using negative contrast in T_2-weighted image has several problems: 1) Extremely high local concentrations of SPIO may produce a complete signal void preventing the accurate quantification of SPIO concentration; 2) The detection of SPIO in regions with low intrinsic signal-to-noise ratio (SNR) is difficult; 3) It is difficult to distinguish field inhomogeneity

induced by SPIO from those caused by air-tissue interfaces, 4) The long echo times required to detect low concentration SPIO causes difficulty in detecting moving objects such as the hearts, where short echo times are optimal ; 5) there are partial volume effect in negative contrast, that is, the ability to detect a void signal depends critically on the resolution of the image.

In order to overcome drawbacks of negative contrast detection, several positive contrast techniques were proposed. Using the negative contrast techniques, the site of contrast agent can be located by the dark signal loss whereas using the positive contrast techniques, contrast agent can be detected by the bright high signal intensity. Those positive contrast techniques can be categorized into 3 groups [3]: Firstly, white marker [1] and gradient echo acquisition for superparamagnetic particles(GRASP) [2] can be categorized into gradient compensation techniques. By this method, positive contrast can be made by introducing intentional background dephasing. To generate the intentional dephasing of background signal, MRI pulse sequence should be manipulated from usual sequence so that the new pulse sequence could make change for the gradient along the slice selection direction. Due to this intentional dephasing, image would become very dark throughout the entire image plane if there were no contrast agent. However, in the region near the contrast agent, the signal would be conserved or bright because the induced dipole field by the contrast agent compensates for the dephasing gradient. Secondly, Inversion recovery on resonance water suppression (IRON) also can be used to make positive contrast image and this method is categorized as an off-resonance techniques. IRON also need pulse sequence manipulation like the white marker. Pulse sequence should be modified so that it could only excite the off resonant protons near the SPIO contrast agent whereas signals originating from on resonant protons are suppressed. The main drawback of gradient compensation techniques (e.g. White marker, GRASP) and Off-resonance techniques (e.g.

IRON) is the need of pulse sequence manipulation since pulse sequence manipulation is a time consuming and tedious job. Thirdly, post processing techniques such as susceptibility gradient mapping (SGM) [3] can generate positive contrast without any modification of pulse sequence, which is the main advantage of the SGM over the other methods. Here the SGM will be described briefly and more detail will be given thoroughly in section 3.5 since SGM motivated phase gradient mapping which is the main topic of this thesis. An object which has different magnetic susceptibility from its surrounding creates a local field inhomogeneity. This field inhomogeneity generates signal loss due to dephasing so we can detect field inhomogeneity using dark area in the T_2 weighted image. However, this field inhomogeneity also can be detected using K-space information since local susceptibility gradient G_{sus} leads to an echo shift in K-space. By measuring this echo shift; which is proportional to the susceptibility gradient, we can make susceptibility gradient map.

2.3 Magnetic susceptibility

2.3.1 Magnetic susceptibility

Magnetic susceptibility is the degree of magnetization of a material in response to an applied magnetic field. For the linear material, magnetization can be defined by

$$M = \chi H \tag{2.1}$$

where M is the magnetization of the material with the unit of $Ampere/meter$ and H is the magnetic field strength, also measured in $Ampere/meter$. Since M and H have same unit, χ should be dimensionless quantity. Also from the relation between B and H , we can get

Table 2.2 Comparison of negative contrast and positive contrast methods for detecting paramagnetic contrast agent.

Name	Category	Idea	Drawbacks
T_2 weighted image (Negative contrast)	Traditional method	Detect signal loss due to dephasing	Many general drawbacks of negative contrast
SGM (Positive contrast)	Post processing technique	Measure echo shift in K-space	Uncertainty from the fitting procedure
White marker (Positive contrast)	Gradient compensation technique	Gradient from the contrast agent compensate the intentional background dephasing	Compensate only for the gradient along slice selection direction Needs of manipulation of pulse sequence
IRON (Positive contrast)	Off resonance technique	Selective excitation of protons near the contrast agent	Needs of prior knowledge about field distribution Needs of manipulation of pulse sequence

$$B = \mu_0(H + M) = \mu_0(1+\chi)H = \mu H = \mu_r \mu_0 H \qquad (2.2)$$

The relation between susceptibility χ and relative permeability μ_r, that is $\chi = \mu_r - 1$, could be obtained and this tell us that magnetic susceptibility and relative permeability is basically same quantity. Materials could be classified by the susceptibility. If χ is positive then the material is called paramagnetic. In the presence of paramagnetic material, the magnetic field is strengthened by the material. If the susceptibility value is negative, then it is called diamagnetic. Diamagnetic material weakens the magnetic field [12].

2.3.2 Induced magnetic field by susceptibility

When an object having susceptibility is placed in the magnetic field, it becomes magnetized and generates an induced magnetic field. In order to get the exact function of induced magnetic field under real situation, differential equations with boundary condition should be solved and this is a very hard task. However, induced magnetic field of an ellipsoidal object can be calculated relatively easily by an algebraic way [12]. This was the contribution of Poisson. Spheres and cylinders are special case of ellipsoids and many practical situations can be approximated by ellipsoids.

2.3.2 Effect of susceptibility on Gradient echo MRI

Gradient echo imaging is very popular pulse sequence in MRI. Gradient echo imaging uses two opposite sign gradients to form an echo. The first gradient accelerates the dephasing of spins and the second gradient with opposite polarity rephase spins to form an echo. The main drawback of gradient echo imaging is the sensitivity of imaging to magnetic field inhomogeneity. Field inhomogeneity can be caused from the presence of ferromagnetic object (ex: metal implant), susceptibility variation at air tissue interfaces, and localized concentrations of hemoglobin in hemorrhage. Shortening the TE can reduce the effect of field inhomogeneity in gradient echo imaging since it minimizes the time in which field inhomogeneity affect to the imaging. The presence of field inhomogeneity can cause two main effects on the gradient echo imaging, image distortion and echo shift [13].

Image distortion

To simplify discussion, only linear local field inhomogeneity will be considered. Since gradient is defined as the spatial slope of magnetic field, i.e. $G = dB / dx$, linear field inhomogeneity

means a constant gradient G along space. The presence of linear field inhomogeneity G' makes the image distorted since the actual gradient during sampling is now $(G+G')$ instead of original gradient G . Let x denote the position of object when there is no field inhomogeneity and x' denote the position of object at the presence of field inhomogeneity. Since the position of MR image is calculated from the measured frequency [13], we can get

$$\gamma\cdot(G+G')\,x' = \gamma\, G\, x \tag{2.3}$$

$$x' = \frac{G}{G+G'}\cdot x = \lambda\cdot x \quad , where \;\; \lambda = \frac{G}{G+G'} \tag{2.4}$$

The scaling factor λ determine the image distortion. If $\lambda < 1$ then image appears stretched and if $\lambda > 1$ then image appears shrunken since the FOV decreases or increases locally.

Echo shift

Field inhomogeneity induced by susceptibility difference can also cause echo shift in K-space. Suppose that the pulse sequence is designed to form an echo at TE, which means that all the spins within a given voxel are rephased again at TE. However, at the presence of field inhomogeneity, the actual time of echo is shifted from the designed TE. The echo shift depends on the polarity of the additional background gradient. If we have positive readout gradient G and negative background gradient G' then the echo is shifted from its ideal position at TE toward longer TE'. In this case, the number of sampling points (q_+) is given by the following equation [13].

$$q_+ = \frac{|G_x'|}{G - |G_x'|}\cdot\frac{TE}{\Delta t} \tag{2.5}$$

On the contrary, for a negative G', the number of sampling point (q_-) can be given by [13]

$$q_- = \frac{G_x'}{G + G_x'} \cdot \frac{TE}{\Delta t} \tag{2.6}$$

If the background gradient is large then it is possible for a signal to be pushed outside the acquisition window and the total signal is lost. So echo shift is one of the main consequences of field inhomogeneity effect and it will be discussed more in the SGM section since echo shift is the heart of SGM.

2.4 White marker and IRON

2.4.1 White marker

White marker [1] is one of the positive contrast techniques. The positive contrast result from the dephasing the background signal with a slice selection gradient.While near the contrast agent the signal is conserved because of the magnetic field induced by the contrast agent. In order to implement this method, pulse sequence manipulation is required since we need a conventional gradient echo imaging with a reduced refocusing RF pulses along slice selection direction. In usual gradient echo imaging sequence, gradient along z direction is used for slice selection. However any gradient during imaging sequence result in the intravoxel dephasing, since spins in the voxel will rotate with different frequencies due to field in homogeneity induce by that gradient. So after the slice selection gradient, a refocusing gradient with opposite polarity is required to prevent signal loss from intravoxel dephasing. As a consequence, gradient echo imaging pulse sequence with reduced refocusing gradient result in signal loss due to dephasing throughout the entire image. However, near the contrast agent, there is an additional gradient

induce by contrast agent which would compensate the signal loss. The signal near the contrast agent is totally compensated by the induced field gradient due to contrast agent, which gives us positive bright signal. Whereas the signal far from the contrast agent is still dark since the signal in that area is not completely compensated. The above explanation about the white marker can be described using Figure 2.1.

2.4.2 IRON

Inversion recovery on resonance water suppression (IRON) [2] is another way of imaging technique which can generate positive contrast. Cell labeled with a SPIO will make a magnetic field surrounding the cell. The induce field can be approximated by a dipole field generated from a magnetized sphere. The ideal dipole field can be described by the following equation [12]

$$\Delta B_z(r,\theta) = \frac{\Delta\chi B_0}{3}\left(\frac{a}{r}\right)^3 (3\cos^2\theta - 1) \qquad (2.7)$$

where $\Delta\chi$ is the susceptibility difference between sphere and surroundings, a is the radius of the sphere, r is the distance from the sphere center, and θ is the angle relative to the main field, B_0. Figure 2.2 below describe the isofrequency contours surrounding a magnetized sphere.

Suppose that we know the information about ideal magnetic sphere such as $\Delta\chi$ and r. Then we can manipulate the MRI pulse sequence by adjusting center frequency and bandwidth of RF pulse so that it only excite the off resonance protons in close vicinity to the SPIO. This selective excitation could produce positive contrast image. However, in order to manipulate MRI pulse sequence for selective excitation, we need prior information for the distribution of contrast agent, which can be one of drawbacks of IRON.

2.5 Post processing method

2.5.1 Susceptibility Gradient Mapping (SGM)

Susceptibility Gradient Mapping (SGM) [3] is a positive contrast imaging method that can be categorized into a post processing technique requiring no pulse sequence manipulation. The SGM method is based on the fact that additional gradients during data acquisition cause an echo shift in K-space. By measuring the echo shift in K-space, the strength of the susceptibility gradients and their direction for each pixel can be determined. This mapping of susceptibility gradients along x, y, and possibly z can be used to make positive contrast image for the SPIO contrast agent. The magnetic field gradient is the core part of the image reconstruction technique in MRI. By encoding spatial information into the signal using phase or frequency gradients, we can reconstruct the image. However if there is an additional gradient which is not designed for spatial encoding, then the echo in K-space is shifted by the amount proportional to the strength of the additional gradient. Since SPIO has a different susceptibility compared to its surroundings, there is a magnetic field gradient around SPIO which causes an echo shift in K-space. The SGM method measures this echo shift and produces a map displaying the magnitude of the shift so that we can generate a positive contrast indicating the field inhomogeneity induced by SPIO.

Echo shift due to gradient induced by susceptibility

The rotational frequency of spin (ω) is proportional to the strength of the magnetic field (B) it is experiencing and is given by the following Larmor equation [5]:

$$\omega = \gamma B, \quad \textit{where } \gamma \textit{ is a gyromagnetic ratio} \tag{2.8}$$

So, if the field within a voxel is inhomogeneous then the group of spins experience a different magnetic field, and so they process out of phase with each other. Since the total magnetization

vector of a voxel is just the sum of each spin magnetization vector, the overall signal from the voxel is lost by canceling out each other. This out of phase precession of spins and resulting signal loss can be referred to as a dephasing of signal. Likewise, a rephrasing of signal refers to the in phase precession of spins and signal recovery. When the signal reaches its maximum value by rephasing, we say that an echo of signal was formed. The idea of gradient echo imaging is to use the gradient of field with opposite polarities. First, the negative gradient accelerates dephasing for the purpose of short echo time (TE). By applying the second positive gradient, spins begin to rotate in the opposite direction and spins become in phase, i.e. they form an echo when the area made by the negative gradient is the same as the area made by the positive gradient. The reason why an echo forms when the two areas are the same can be explained by the following. Let ϕ be the rotation angle of spin, then ϕ can be expressed as

$$\begin{aligned} \phi &= \omega t \qquad (\omega : angular\ velocity) \\ &= \gamma B t \qquad (\because\ \omega = \gamma B) \\ &= \gamma G x t \qquad (\because\ B = Gx) \end{aligned} \tag{2.9}$$

Equation (2.9) indicates that in the G versus x graph, the area ($G \cdot x$) is proportional to the rotational angle ϕ of spin. The echo forms when the area made by two positive and negative lobes is the same, which means the rotation angle of all spins are identical. However, additional gradients make the echo move from the center to a new point at which the two areas including additional gradients are equal. (See Figure 2.3).

Derivation of equation for echo shift due to susceptibility

The relation between echo shift in K-space and gradients induced by susceptibility (G_x^{sus}) can be derived. We will only consider the linear part of a field inhomogeneity as a first order

approximation. Since the gradient is the spatial slope of the magnetic field, linear approximation of field inhomogeneity corresponds to the constant susceptibility gradient (G_x^{sus}) through space. The measured signal along the readout direction can be written as [14]

$$S(t) = \sum_{n=0}^{N-1} \rho(n \quad \Delta x)\, e^{-i2\pi\ \gamma\ G_x^{imaging} t\ n\ \Delta x}\ e^{-i\ \ \pi\ \gamma \cdot G_x^{sus} \cdot (t+TE) \cdot n\ \Delta x} \tag{2.10}$$

where $\rho(n\Delta X)$ is the spin density and Δx is the pixel size. The phase distortion in the image results from various sources. First, imaging gradient ($G^{imaging}$), which is designed for the specific pulse sequence, can cause a phase change in the image space. Second, gradient induced by susceptibility effect (G^{sus}) can also result in phase change even though this effect was not designed for the imaging. Third, coil sensitivity or eddy currents also cause phase changes.

However, we will ignore the third source of phase change for simplicity. Therefore, we only have $G^{imaging}$ and G^{sus} in the equation as our source of phase distortion. Since we have the additional gradient G^{sus} other than the designed gradient $G^{imaging}$, the echo in K-space is shifted. The shifted echo is formed when the effect of the additional susceptibility gradient is completely cancelled by the imaging gradient. Suppose that the shifted echo occurs at time $t = m\tau_x$ then the total phase should be zero at that time. This leads to the following equation:

$$-2\pi\gamma G_x^{imaging} m\tau_x n\Delta x - 2\pi\gamma G_x^{sus}(m\tau_x + TE)n\Delta x = 0 \tag{2.11}$$

which leads to

$$m = -\frac{G_x^{sus} TE}{(G_x^{imaging} + G_x^{sus})\tau_x} \tag{2.12}$$

where $1/\tau_x$ is the sampling rate.

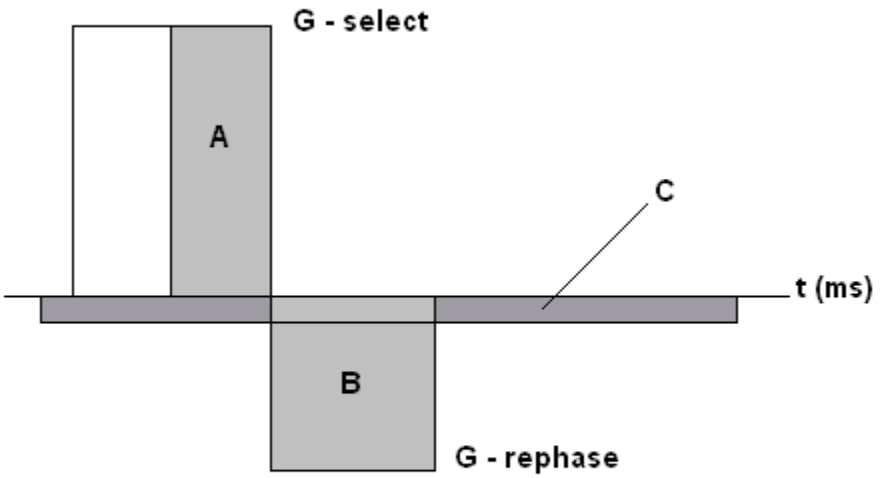

Figure 2.1 White marker: schematic depiction of the concept of signal conservation for gradient areas in the slice selection direction. In general, after excitation at t=0 msec, the slice selection gradient dephases (area A) the spins. To rephase the excited spins, normally the full area B compensates for the slice selection area. Reducing area B creates a gradient imbalance, effectively resulting in a signal decrease. However, in spatial regions with a negative local gradient due to the dipole field (area C), the gradient balance is restored and the signal remains conserved, whereas other regions will experience signal loss.

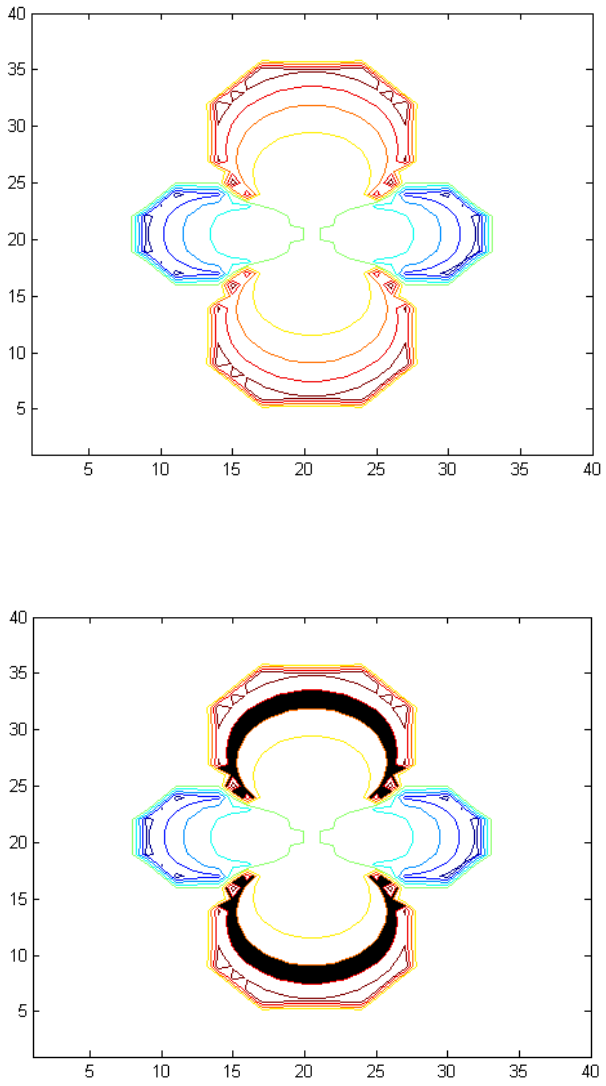

Figure 2.2 IRON: Isofrequency contours surrounding a magnetized sphere are shown, with the shaded regions showing the spatial extent of the regions that would be excited by a band – selective RF pulse. (From [2])

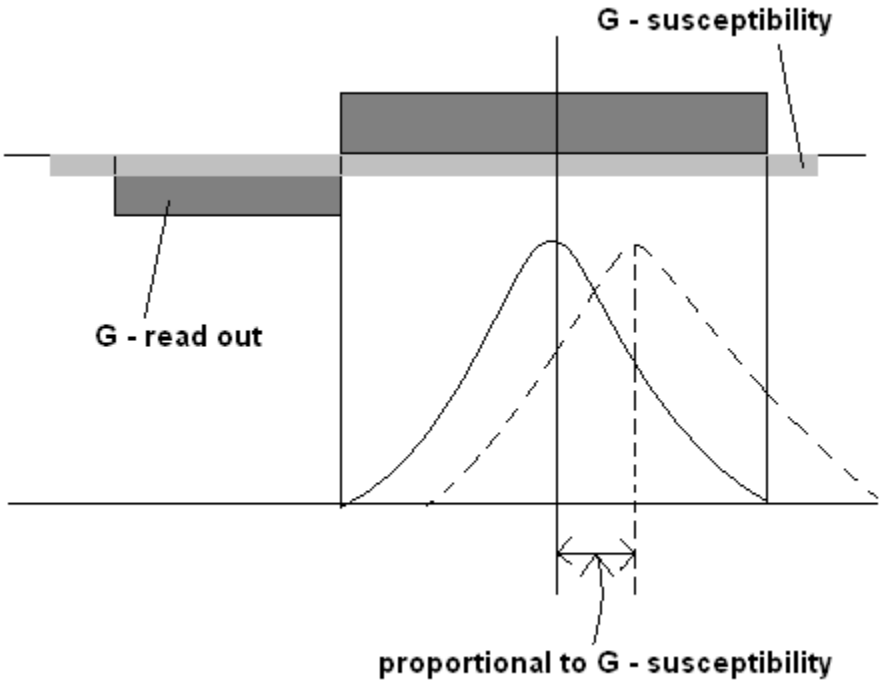

Figure 2.3 Illustration of the SGM. By the susceptibility effect, SPIO produce local magnetic field gradient G_{suscep}. Without this G_{suscep}, echo is formed at the peak point indicated by the solid line. However, in the presence of G_{suscep}, the echo is formed at the peak point indicated by the dotted line. This echo shift is proportional to the strength of G_{suscep},which is given by equation (2.12). Basically, SGM measures this echo shift in k-space as an indication of presence of susceptibility gradient.

Fourier shift theorem connect phase slope in image and echo shift in K-space

The echo in K-space is shifted by gradient induced by susceptibility as mentioned above. That echo shift in K-space is related to the slope of phase in image through the Fourier shift theorem. Let $S(k)$ be the signal in k-space and $\hat{\rho}(x)$ be the complex reconstructed image from $S(k)$. Consider a signal $S(k-k_0)$ which is shifted in k-space by k_0. Then the complex image $\hat{\rho}_{k-k_0}(x)$ reconstructed from $S(k-k_0)$ is given by [5]

$$\begin{aligned}\hat{\rho}_{k-k_0}(x) &= F^{-1}\left[S(k-k_0)\right] \\ &= e^{i2\pi k_0 x}\,\hat{\rho}_k(x)\end{aligned} \tag{2.13}$$

Equation (2.13) is referred to as the Fourier shift theorem and implies that the shift in k-space (k_0) induces a linear phase change ($2\pi k_0 x$) in the reconstructed image $\hat{\rho}_k(x)$. In fact, this Fourier shift theorem provide the theoretical background for the phase gradient mapping method which will be discussed in a later chapter. Notice that even though there is a phase change in the image reconstructed from the shifted k-space signal, the amplitude is the same as the image reconstructed from the unshifted image since

$$\left|\hat{\rho}_{k-k_0}\right| = \left|e^{i2\pi k_0 x}\hat{\rho}_k\right| = \left|e^{i2\pi k_0 x}\right|\cdot\left|\hat{\rho}_k\right| = 1\left|\hat{\rho}_k\right| = \left|\hat{\rho}_k\right| \tag{2.14}$$

Calculating echo shift in K-space

The susceptibility gradient (G^{sus}) along x, y, and z for each voxel can be determined by performing a 1D FFT over a subset of n neighboring voxels along the x,y,and z direction, respectively. After 1D FFT, n discrete Fourier component was fitted using the quadratic equation.

The echo shift can be measured using the distance between the origin and the maximum point of a quadratic fitting curve. Since echo shift is proportional to the gradient induced by a susceptibility difference, echo shift map is equivalent to the susceptibility gradient map.

2.5.2 The energy spectrum method

An object with a different magnetic susceptibility from its surroundings produces a magnetic field and this induced field inhomogeneity can cause image distortion and echo shift. Basically, SGM measures this echo shift in k-space generated by field inhomogeneity. By mapping the echo shift of each voxel, we can get a susceptibility map, since susceptibility introduces echo shift. Energy spectrum method [4] is another way of measuring echo shift in k-space. In this method, K-space lines are subsequently truncated and zero filled. First, most bottom line of K-space is deleted and filled with zeroes. This truncated K-space is transformed to the image using 2 dimensional Fourier transformations as usual. Then signal intensities of all voxels in the image are recorded. This procedure is continued line by line. If the truncation and zero filling are repeated from the bottom most line to top most line, signal intensity of each voxel through truncation can be obtained. Figure 2.4 shows the typical patterns of signal intensity plot along x direction. For a 3D dataset, truncation can be performed in all dimensions x,y,and z respectively. In both voxels, there is a point of truncation where signal intensity drops suddenly. Basically, the number of truncation along K_x lines indicates the x coordinate in K-space. So a sudden change in signal intensity of a voxel means that we just deleted the echo correspond to the voxel. In other words, since we removed the part of K-space which mostly contributes to the signal intensity of that voxel, the signal drops significantly at the point of the truncation. If there is no field inhomogeneity generated by susceptibility differences in a certain voxel, the sudden change

should occur at the center of K-space, since in that case echo should be at the center of K-space (Solid line in Figure 2.4). If there is a susceptibility effect at a certain voxel, then the point of sudden drop should be shifted since the echo corresponding to that voxel is shifted by the effect of field inhomogeneity (Dotted line in 2.4). Therefore, by measuring the K-space line at which a sudden drop of signal intensity occurs for every voxel, the shift in K-space for each voxel can be determined.

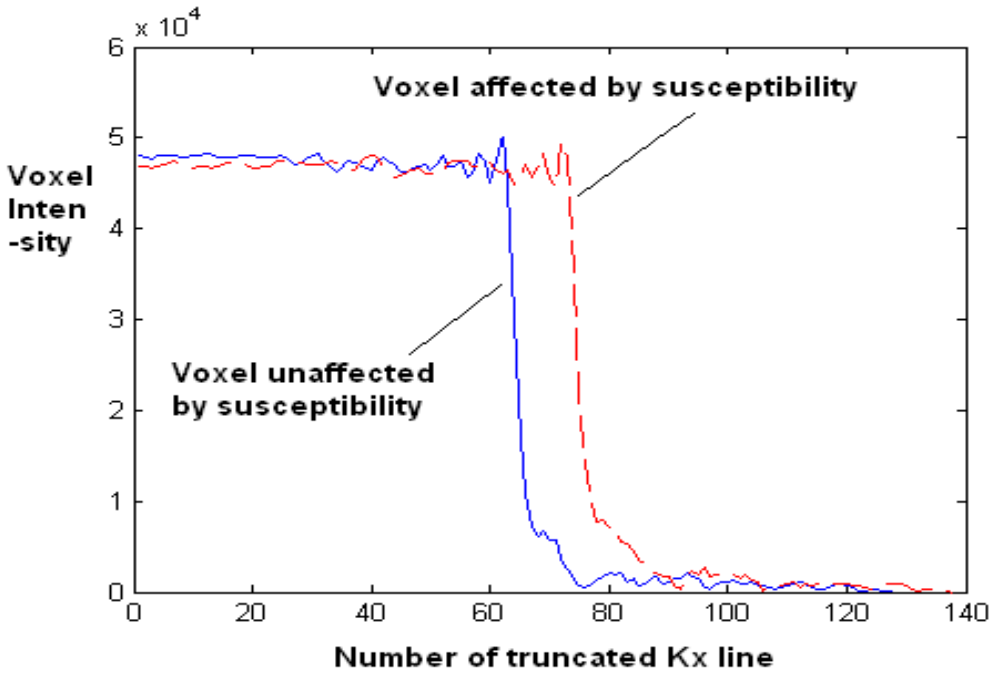

Figure 2.4 Illustration of the energy spectrum method. Signal intensity variation of two voxels along K_x truncation. The solid line represents the signal intensity variation from the voxel which is not affected by susceptibility and the dotted line represents the signal intensity variation from the voxel which is affected by susceptibility. The sudden drop of signal intensity indicates the echo in K-space is just removed by deleting the K-space line, which lets us know the location of the echo corresponding to that voxel. With no susceptibility effect, echo is located at the center of K-space. However, the echo is shifted by the susceptibility effect.

2.5.3 Phase gradient mapping

Tracking of the paramagnetic contrast agent in vivo can be used in many areas and traditional T_2 weighted images can show us negative contrasts for the paramagnetic contrast agent. Since there are many drawbacks to negative contrast, various positive contrast methods were proposed such as IRON, White marker, and SGM. Among them, SGM measures echo shift in K-space, which is generated from the susceptibility gradient. The main advantage of SGM is that it doesn't require manipulation of pulse sequences, which would need a lot of effort. However, the measuring of echo shift in K-space needs a fitting procedure which results in inherent uncertainty in SGM. In fact, the Fourier shift theorem tells us that echo shift in K-space is equivalent to the phase change (i.e. slope of phase map) in image space.

The reason why other methods such as SGM were trying to measure echo shift instead of phase slope is that wrapping in the phase map prevents us from measuring slope correctly. Phase gradient mapping is a method for measuring the slope of the phase map in spite of the presence of wrapping in the phase map. Since phase gradient mapping doesn't require any fitting procedure, it should be a more accurate measure of the susceptibility gradient than SGM. In fact, the phase gradient mapping uses some calculation methods of the proposed unwrapping algorithm which is called moment based unwrapping method [15]. The following are more detailed theoretical description of phase gradient mapping. Suppose that $\rho(x, y)$ is the complex number whose magnitude represents length of the magnetization vector and whose angle represents phase angle of the magnetization vector:

$$
\begin{aligned}
& \rho(x,y) = \left|\rho(x,y)\right| e^{i\phi(x,y)} \\
\Rightarrow \quad & \frac{\rho(x,y)}{\left|\rho(x,y)\right|} = e^{i\phi(x,y)} \equiv \bar{\rho}(x,y) && (\textit{devide } \rho(x,y) \textit{ by } \left|\rho(x,y)\right|) \\
\Rightarrow \quad & \frac{\partial \bar{\rho}(x,y)}{\partial x} = i\, e^{i\phi(x,y)} \frac{\partial \phi(x,y)}{\partial x} && (\textit{take the derivative of } \bar{\rho}(x,y)) \\
\Rightarrow \quad & \frac{\partial \phi(x,y)}{\partial x} = -i\, e^{-i\phi(x,y)} \frac{\partial \bar{\rho}(x,y)}{\partial x} && (2.15) \\
& = -i\, \bar{\rho}^{*}(x,y) \frac{\partial \bar{\rho}(x,y)}{\partial x} && (\textit{where } \bar{\rho}^{*}(x,y) \textit{ represents} \\
& && \textit{complex conjugate of } \bar{\rho}(x,y))
\end{aligned}
$$

We can do the same thing with respect to y so that we have two equations :

$$\frac{\partial \phi(x,y)}{\partial x} = -i\, \bar{\rho}^{*}(x,y) \frac{\partial \bar{\rho}(x,y)}{\partial x} \qquad (2.16)$$

$$\frac{\partial \phi(x,y)}{\partial y} = -i\, \bar{\rho}^{*}(x,y) \frac{\partial \bar{\rho}(x,y)}{\partial y} \qquad (2.17)$$

Equation (2.16) and (2.17) can be used to get $\frac{\partial \phi(x,y)}{\partial x}$ and $\frac{\partial \phi(x,y)}{\partial y}$,which are the spatial derivatives of the phase map. As it was indicated that the echo shift in k-space is equivalent to the phase change in the image space. SGM measures echo shift in K-space to detect a susceptibility gradient. So we can conclude that the phase change (or slope of phase) in image space can be used to detect the susceptibility gradient and equations (2.16) and (2.17) guarantee that we can calculate $\frac{\partial \phi(x,y)}{\partial x}$ and $\frac{\partial \phi(x,y)}{\partial y}$ without worrying about phase unwrapping. In equation (2.16) and (2.17), we can easily get $\bar{\rho}\ (x,y) = \frac{\rho(x,y)}{\left|\rho(x,y)\right|}$ by simply normalizing $\rho(x,y)$.

In summary, we can use (2.16) and (2.17) to get $\frac{\partial\phi(x,y)}{\partial x}$ and $\frac{\partial\phi(x,y)}{\partial y}$ which are equivalent to the echo shift in K-space by the Fourier shift theorem. By calculating $\frac{\partial\phi(x,y)}{\partial x}$ and $\frac{\partial\phi(x,y)}{\partial y}$ instead of echo shift, we can also get the information about field inhomogeneity due to susceptibility.

2.6 Methods and Results

Data

Phantom data

A phantom was made in the lab by filling an acrylic cylinder (20cm in diameter) with agarose gel (33g agar/1000ml water) to simulate human tissue. Three plastic cylinder vials (1cm in diameter) which contain iron oxide (Fe_2O_3) nano particles in the enclosed gel were embedded into the large, cylindrical phantom. Experimental MR measurements were taken using a 3.0 T GE SIGNA HDX MR scanner (GE Medical Systems, Milwaukee, WI). Gradient refocused echo (GRE) scans were taken on the phantom (see Figure 2.5 a). An image was obtained using the following parameters, TE=7 ms, TR=150 ms, Flip angle = 90 degree, and 128*128 matrix.

In vivo Mouse data

Mouse data were taken using a Philip Achieva clinical MR scanner. 36 slices of mouse were scanned and stored as a DICOM format. The images were scanned using a three-dimensional fast field echo sequence (3DFFE) with 256x256 matrix size, slice thickness = 0.7mm, and FOV = 70mm*70mm. Inside the mouse, there are two tumor areas labeled with SPIO nano particles (see Figure 2.5 b).

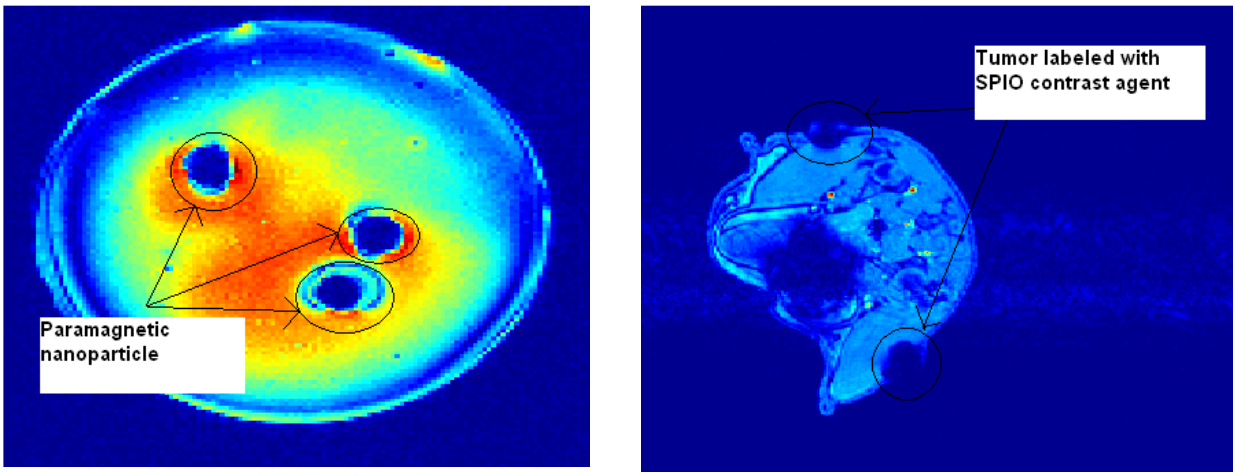

a b

Figure 2.5 a) Phantom was made using agaros gel. 3 cylinders containing paramagnetic iron are embedded into the agaros gel. b) Mouse with tumor labeled with SPIO nano particle.

Method for SGM

SGM measures the echo shift in K-space. The echo shift ($m_{x,y}$) was calculated using gradient echo (GRE) data for phantom and three-dimensional fast field echo sequence (3D-FFE) data for mouse. First, for every voxel in the image, n (here n=8) neighboring voxels along x direction were chosen as a subset. A 1-D Fourier transform was applied to get the k-space information of that subset. The result of 1-D Fourier transform was n (here n=8) discrete data points in k-space and these points were fitted using a quadratic function. A *sinc* function may be more appropriate for the k-space data, but sinc function fitting needs many data points. Therefore, a quadratic

function was used as the approximation of sinc function fitting. From the fitted quadratic curve for the k-space data, the maximum point of that curve was calculated. The echo shift of that voxel can be calculated from the distance between the maximum point of the quadratic function and the origin as seen in Figure 2.6.

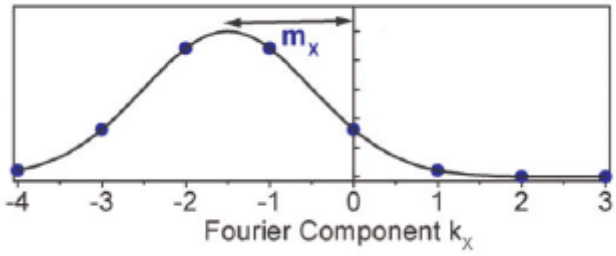

Figure 2.6 Echo shift of a voxel is the difference between the maximum point of quadratic fitting and the origin. (Image is from [14])

This procedure can be repeated and echo shift ($m_{x,y}$) can be assigned to every voxel. Since the magnitude of the vector ($m_{x,y}$) is proportional to the strength of the susceptibility gradient [14],

$$m = -\frac{G_x^{sus} TE}{(G_x^{imaging} + G_x^{sus})\tau_x} \qquad (2.18)$$

the map of magnitude of $m_{x,y}$ generates an image which makes the areas of strong changes in susceptibility positively highlighted. All data analysis was performed using MATLAB 2006b. For the 1D Fourier transformation, the MATLAB built-in fft function was used. Also for the quadratic fitting, the MATLAB built-in polyfit function was used

Uncertainty analysis for SGM

In SGM, we need a quadratic fitting to calculate echo shift. Echo shift can be expressed as the function of parameters estimated from a quadratic fitting, i.e. echo shift = $-B/2A$, where A, B are the coefficient of $Ax^2 + Bx + C$. Estimated parameters from any fitting procedure always have a certain degree of uncertainty and that uncertainty is usually provided as a form of confidence interval. The uncertainty of estimated parameters in quadratic fitting would propagate into echo shift. Propagation of error method [16] is a systematic way for analyzing such error transfer. It gives us the following formula regarding uncertainty of echo shift.

$$\left(\frac{\sigma_{echo\ shift}}{echo\ shift}\right)^2 = \left(\frac{\sigma_A}{A}\right)^2 + \left(\frac{\sigma_B}{B}\right)^2 \qquad (2.19)$$

Equation (2.22) can be derived as the following: suppose that we have a quadratic function, say $Ax^2 + Bx + C$, then echo shift is just the axis of that quadratic function, i.e. echo shift = -B/2A = $f(A,B)$. We can expand $f(A,B)$ using a Taylor series centered at (μ_A, μ_B)

$$f(A,B) = f(\mu_A,\mu_B) + (A-\mu_A)\frac{\partial f}{\partial A}\bigg|_{\mu_A,\mu_B} + (B-\mu_B)\frac{\partial f}{\partial B}\bigg|_{\mu_A,\mu_B} + higher\ order\ terms$$

If we assume that the measured values are close to the average values then we can ignore the higher order terms. Now let's consider the variance of $f(A,B)$,which is our quantity of interest.

$$\begin{aligned} Var[f(A,B)] &= Var[f(\mu_A,\mu_B) + (A-\mu_A)\frac{\partial f}{\partial A} + (B-\mu_B)\frac{\partial f}{\partial B}] \\ &= Var[\frac{\partial f}{\partial A}A + \frac{\partial f}{\partial B}B] \qquad (\because Var[const] = 0) \\ &= \left(\frac{\partial f}{\partial A}\right)^2 Var[A] + \left(\frac{\partial f}{\partial B}\right)^2 Var[B] + \frac{\partial f}{\partial A}\frac{\partial f}{\partial B}Cov[A,B] \end{aligned}$$

If we assume $Cov[A,B]=0$, then we have

$$Var[f(A,B)]=\left(\frac{\partial f}{\partial A}\right)^2 Var[A]+\left(\frac{\partial f}{\partial B}\right)^2 Var[B]$$

Since echo-shift can be expressed as a function of parameters A and B, i.e. echo shift = $f(A,B)=-B/2A$, we would have

$$\begin{aligned} Var[Echo-shift] &= Var[f(A,B)] \\ &= \left(\frac{\partial f}{\partial A}\right)^2 Var[A]+\left(\frac{\partial f}{\partial B}\right)^2 Var[B] \quad (\because \textit{from above}) \\ &= \frac{B^2}{4A^4}Var[A]+\frac{1}{4A^2}Var[B] \quad (\because \frac{\partial f}{\partial A}=\frac{B}{2A^2}, \frac{\partial f}{\partial B}=-\frac{1}{2A}) \end{aligned}$$

Finally, by dividing both side with $B^2/4A^2$, we get

$$\begin{aligned} & \frac{Var[f(A,B)]}{\left(\frac{B^2}{4A^2}\right)}=\frac{Var[A]}{A^2}+\frac{Var[B]}{B^2} \\ \Rightarrow \quad & \frac{Var[f(A,B)]}{(Echo-shift)^2}=\frac{Var[A]}{A^2}+\frac{Var[B]}{B^2} \\ \Rightarrow \quad & \left(\frac{\sigma_{echo\,shift}}{echo\,shift}\right)^2=\left(\frac{\sigma_A}{A}\right)^2+\left(\frac{\sigma_B}{B}\right)^2 \end{aligned}$$

Method for Phase gradient mapping (PGM)

For the PGM method, a 2D phase map calculation of the $\partial\varphi(x,y)/\partial x$ and $\partial\varphi(x,y)/\partial y$ was implemented by performing a Fourier Transform directly on the phase image, row by row for $\partial\varphi(x,y)/\partial x$, and column by column for $\partial\varphi(x,y)/\partial y$, without unwrapping the 2D phase image. Note that this is a one-step procedure to acquire the phase gradient, as compared to the SGM method where a variable size sliding window was applied first and followed by a quadratic curve fitting procedure. In a 3D phase map, phase derivatives along x-, y-, and z-directions were implemented by performing a Fourier Transform directly on the 3D phase image, row by row for $\partial\varphi(x,y,z)/\partial x$, column by column for $\partial\varphi(x,y,z)/\partial y$, and column by column in the z-direction for $\partial\varphi(x,y,z)/\partial z$, without unwrapping the 3D phase image. A PGM map is obtained by combining those three components into one using $\sqrt{(\partial\varphi/\partial x)^2+(\partial\varphi/\partial y)^2+(\partial\varphi/\partial z)^2}$.

As a comparison to the phase gradient mapping which does not need a phase unwrapping procedure, a direct phase derivative on the phase image (wrapped) is also calculated using a MATLAB function. A final combined image $\sqrt{(\partial\varphi/\partial x)^2+(\partial\varphi/\partial y)^2+(\partial\varphi/\partial z)^2}$ is demonstrated to show the results.

Results

Phantom data set

Results of the Phase gradient mapping (PGM), Susceptibility gradient mapping (SGM), and direct phase derivatives were presented in Figure2.7. Since the data for the phantom was obtained using a 2D imaging sequence, only x and y direction results were combined to make a positive contrast map. PGM (Figure 2.7.a) and SGM (Figure 2.7.b) both show clear positive contrasts around three SPIO vials. In the direct phase derivative (Figure 2.7.c), gradients along

wrapped phase areas were also detected, in addition to the three SPIO vials. It was also noted that the PGM presented multiple ring-shaped contrast surrounding the SPIO vials and along the boundary of the large cylinder. This resulted from the Gibbs ring effect of the Fourier transform of sharp edges, and can be removed partly by masking the data with a Hanning or Hamming window before the Fourier transform.

In vivo Mouse data

Results of the mouse data also show similar results to that of the phantom data above. Phase gradient mapping (PGM), Susceptibility gradient mapping (SGM), and direct phase derivatives were presented in Figure 2.8. For mouse data, an image was obtained using 3D FFE pulse sequence. Therefore, all three x,y, and z direction results were combined to make the final image. It is seen that in the phase gradient mapping (Figure 2.8.a), the two SPIO labeled tumor areas were clearly detected, as well as by the SGM in Figure (Figure 2.8.b). It is seen that the PGM is more sensitive to the field inhomogeneity than the SGM since more positive contrast areas are shown by the PGM. In the direct phase derivative in Figure 2.8.c, gradients along wrapped phase areas were also detected, besides the labeled tumor area. All three methods found the boundary of the mouse tumor, which has smaller susceptibility gradients.

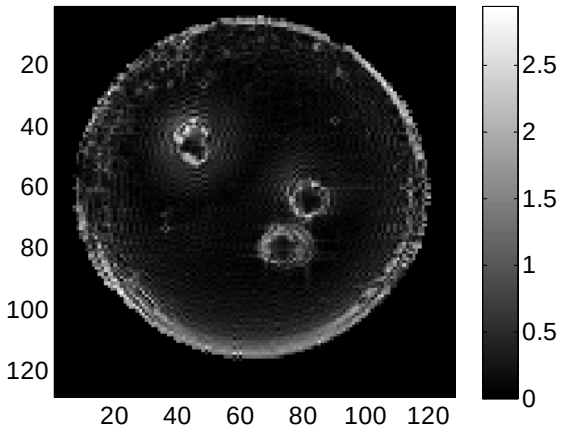

a. PGM for phantom

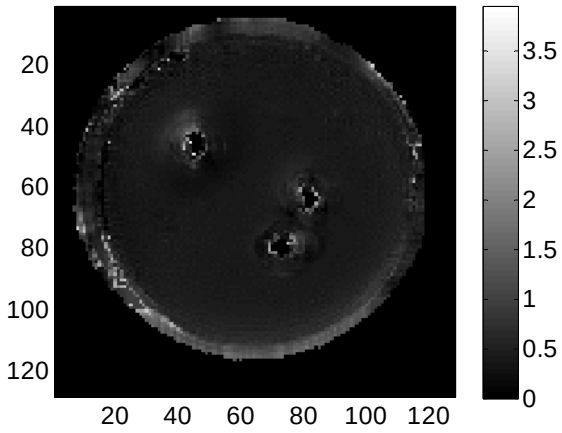

b. SGM for phantom

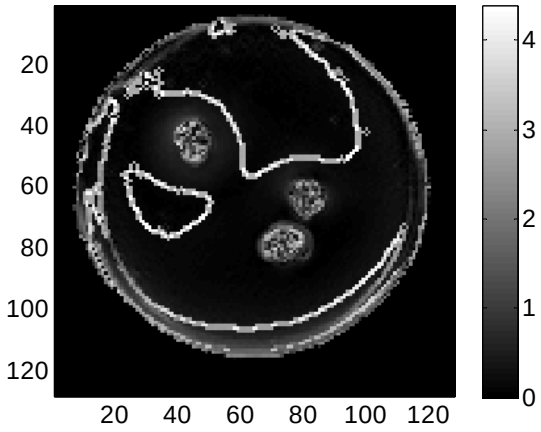

c. Direct derivative of phase map

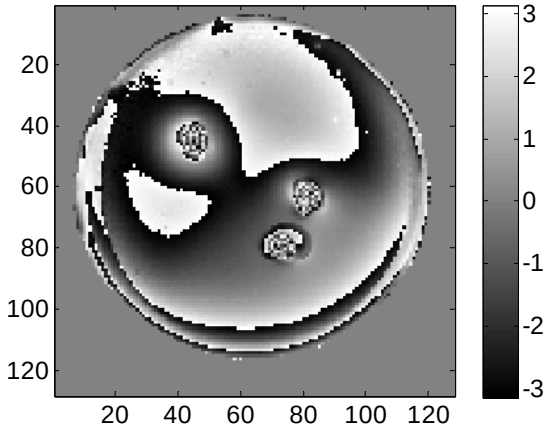

d. Phase map of phantom

Figure 2.7 PGM, SGM, and direct derivative of phantom data

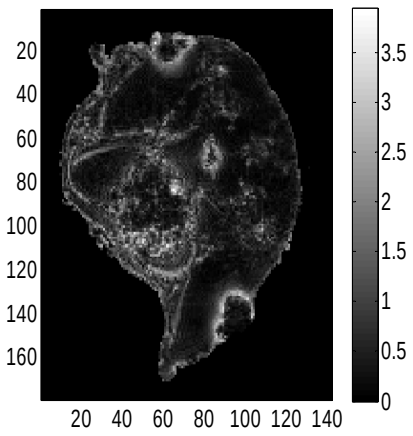

a. PGM for mouse

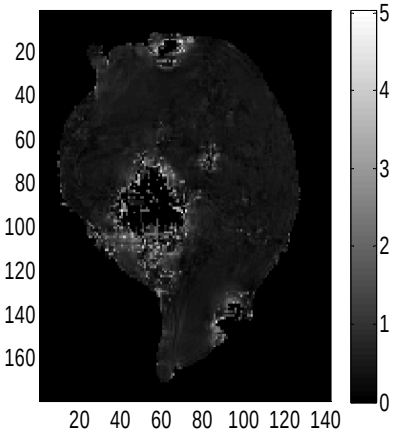

b. SGM for mouse

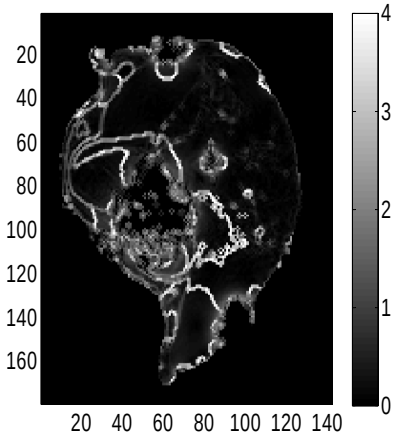

c. Direct phase derivative

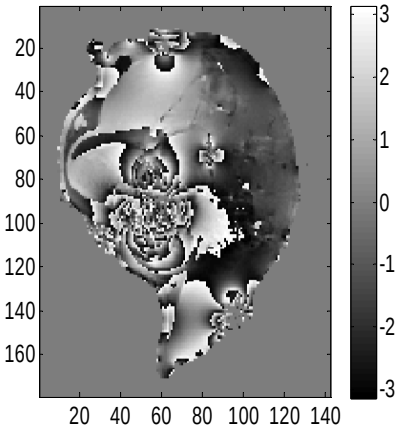

d. Phase map

Figure 2.8 PGM, SGM, and direct derivative of mouse data

Uncertainty of SGM

A quadratic fitting procedure is needed during SGM, which introduces uncertainty in estimating echo shift. Based on the equation (2.19), uncertainties of echo shift from the phantom data were presented in Figure2.9. Figure2.9 (a) and Figure2.9 (b) demonstrate the histogram of echo shift uncertainty ($\sigma_{echoshift}$) for phantom data along x- and y-directions, respectively. The mean values of echo shift uncertainty were 0.8998 (pixels) along the x-direction and 0.8373 (pixels) along the y-direction. Figure 2.10 shows the histogram of echo shift uncertainty for the mouse tumor data in the x-, y-, and z-direction. The mean (and standard deviation) of the uncertainty estimate are shown in Table 2.3. It is seen that the mean uncertainty is less than one pixel but more than half of a pixel. In the mouse tumor data, uncertainty in the z-direction is also bigger than the other two directions.

Table 2.3 Uncertainty measurement using Equation (2.22) for phantom and mouse tumor data

Uncertainty measurement Mean/standard deviation (pixel)	x-direction	y-direction	z-direction
Phantom data	0.8998 ± 0.2682	0.8373 ± 0.2809	N/A
Mouse tumor data	0.8130 ± 0.5213	0.8235 ± 0.5952	0.9219 ± 0.7597

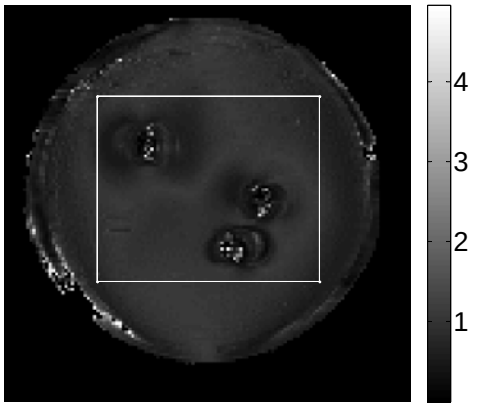

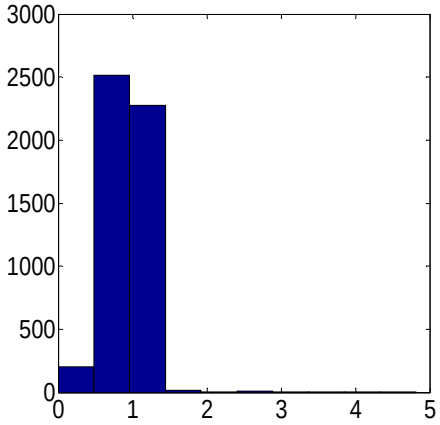

a. Uncertainty map for echoshift along x

b. Histogram Mean=0.8998

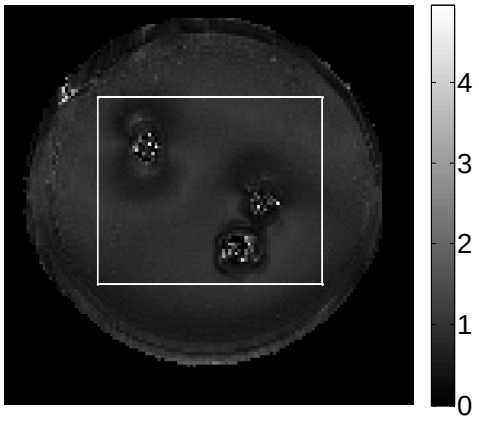

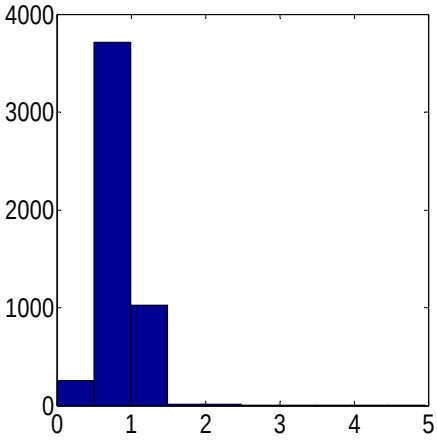

c. Uncertainty map for echoshift along y

d. Histogram Mean=0.8373

Figure 2.9. Uncertainty map associated with echo shift along x- (a) and y-direction (c). The uncertainty was estimated using equation (2.22). Histograms of the uncertainty numbers were extracted from an area (30:100, 30:100) – indicated by white box - in (a) and (c), shown in (b) and (d), respectively.

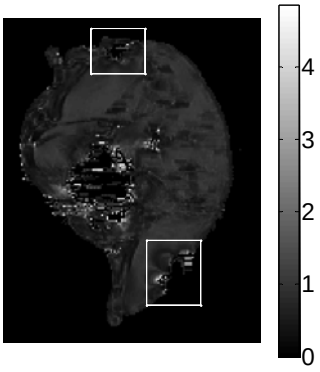

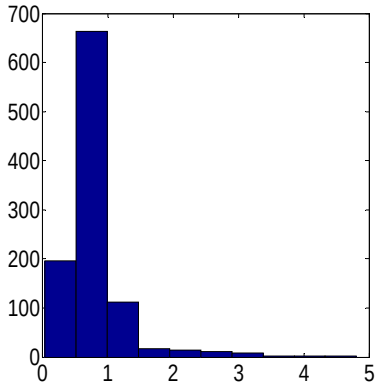

a. Uncertainty along

b. Mean of uncertainty = 0.8130

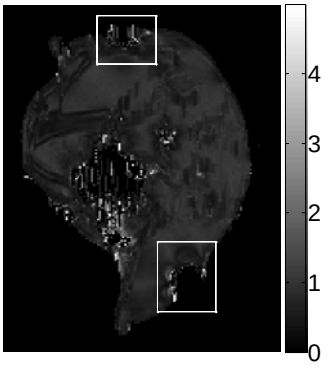

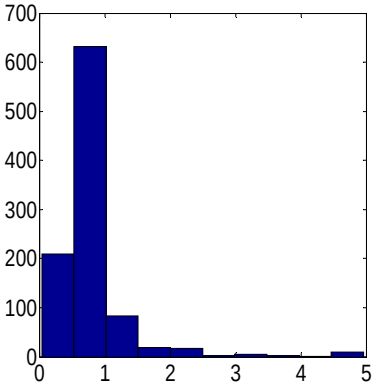

c. Uncertainty along Y

d. Mean of uncertainty = 0.8235

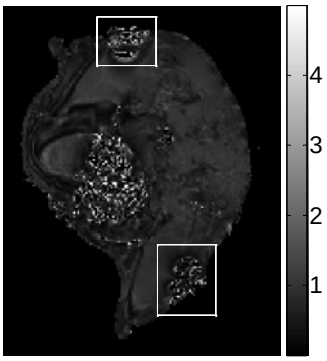

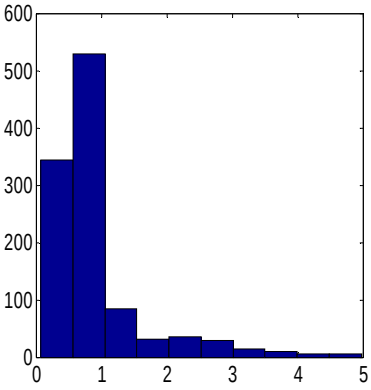

e. Uncertainty along z

f. Mean of uncertainty = 0.9219

Figure 2.10 Uncertainty estimate for the mouse tumor data

2.7 Discussion

Phase gradient mapping (PGM) and susceptibility gradient mapping (SGM) both showed similar positive contrast maps as seen in Figure 2.7 and Figure 2.7. However, there exist differences as well. First, PGM measures the slope of the phase map in the image space whereas SGM uses the echo shift in k-space. In fact, they are equivalent through the Fourier shift theorem (see section 2.5.3). However, the use of the slope of phase map as a positive contrast technique was hampered by the presence of wrapping in the phase map. Since wrapping in the phase map almost always exists in MR imaging, a direct derivative of the phase map shows undesirable line patterns as seen in Figure2.7 (c) and Figure 2.8 (c). PGM can calculate the slope of phase without being concerned with wrapping.

Second, PGM seems more sensitive to small susceptibility gradient than SGM. The SGM uses a sliding window (say, size of n) moving across the complex image and finds out echo shifts for each voxel in the k-space by doing a Fourier transform on the subset covered by the sliding window, which is then followed by a curve fitting. In contrast, the PGM calculates the first derivative of phase, which is equivalent to an echo shift in the k-space, through a Fourier transform on a whole row or column (with size of *N*, and $N>n$) of a phase map. For a certain choice of window size *n*, the measured shift is represented as [17] $m'_{shift} = m_{shift} \cdot n/N$, where m_{shift} is the actual echo shift induced by the susceptibility gradient in x-, y-, or z-direction. . It is easily seen that the window size *n* changes the output of the method. Larger values of *n* may increase the resolution in k-space and therefore can find out smaller local susceptibility gradients. Smaller values of *n* may decrease the resolution in k-space and therefore only pick up larger susceptibility gradients. For the PGM method, the Fourier transform with size *N* performed on a

row or column of a phase map may equivalently have a higher resolution in the k-space than the SGM method so the smaller local susceptibility gradients are likely to be detected. This is shown in Figure 2.8 that area other than the SPIOs, such as the boundary of air/tissue interface, signal void in the center of mouse data phase map, show also positive contrast.

Third, SGM has an inherent uncertainty in measuring echo shift. A fitting procedure is required in SGM to find out maximum echo. Since any fitting procedure has a certain amount of uncertainty in estimating parameters, echo shift measure by SGM should also have uncertainty. The uncertainty of echo shift propagated from the uncertainty of parameters of a quadratic function is calculated using equation (2.19) and presented in Table 2.3, Figure 2.9, and Figure 2.10. This kind of uncertainty does not exist in PGM since PGM does not use any fitting procedure.

Both PGM and SGM could detect well three vials containing the SPIO in the phantom and the tumor labeled with SPIO in the mouse. However, they also detect an area other than SPIO (e.g. air/tissue interface). Therefore, further efforts should be made to differentiate SPIO labeled areas from other area.

CHAPTER 3. DCE MRI

3.1 Introduction

Dynamic contrast enhanced MRI (DCE MRI) [18] is an imaging technique which can be used to investigate the physiology of tissue microvasculature. For DCE MRI, a series of MRI images were taken before, during, and after the injection of an MR contrast agent. Conventional MR imaging can be considered as a snapshot at a given time whereas DCE MRI can be thought of as a movie which is a series of images. From the analysis of time series data of DCE MRI, information about blood volume and vascular permeability ,which are physiological parameters associated with the tumor, can be obtained [19]. DCE MRI is a promising tool for many applications including cancer detection, diagnosis, staging, and assessment of antiangiogenic treatment.

3.2 Theory

3.2.1 Pharmacokinetic model

A pharmacokinetic model is used to estimate parameters such as blood volume and permeability which are associated with the tumor. A pharmacokinetic model refers to the model dealing with the process by which a drug is absorbed, distributed, metabolized, and eliminated by the body. The accuracy of DCE MRI highly depends on the pharmacokinetic models. Physiological parameters which can be estimated from DCE MRI were defined and standardized by Tofts et al [20].

Commonly used pharmacokinetic model only consider contrast agent exchanges between two compartments: the vascular space (plasma) and the EES. This model is called a two-compartment model. In this model, contrast agent enters through the vascular space (central compartment in Figure 3.2 below) by perfusion, and diffuses between the vascular space and EES tumor (peripheral compartment in Figure 3.2 below). The rates of diffusion from the vascular space to the EES are determined by the concentrations of contrast agent in plasma and EES and the permeability of the capillary.

Tofts [20] proposed a differential equation for this two compartment model,

$$\frac{dC_{tumor}}{dt} = K^{trans} C_p - k_{ep} C_{tumor} \qquad (3.1)$$

, where C_{tumor} and C_p are the concentration of the contrast agent in the EES and plasma space. K^{trans} is the transfer constant between the plasma and the EES, and $k_{ep} = K^{trans} / v_e$, where v_e is the fraction of tumor volume occupied by the EES. Thus, the concentration of contrast agent within the tumor is determined by the blood plasma concentration and two parameters, K^{trans}, the transfer constant, and the EES fractional volume index, v_e.

3.2.2 Physiological parameters and tumor

Basically, DEC MRI detects the abnormality of tumor microvasculature. There is a difference between tumor cells and normal cells. In order for tumor cells to grow quickly, they must stimulate the production of blood vessels. Tumor cells start to become dependent on blood supply carried out by neovasculature for their nutritional and oxygen supply. These newly

formed tumor vessels are usually abnormal in form and architecture. This will lead to abnormal molecular and fluid transport dynamics, especially for macromolecular drugs. The network of

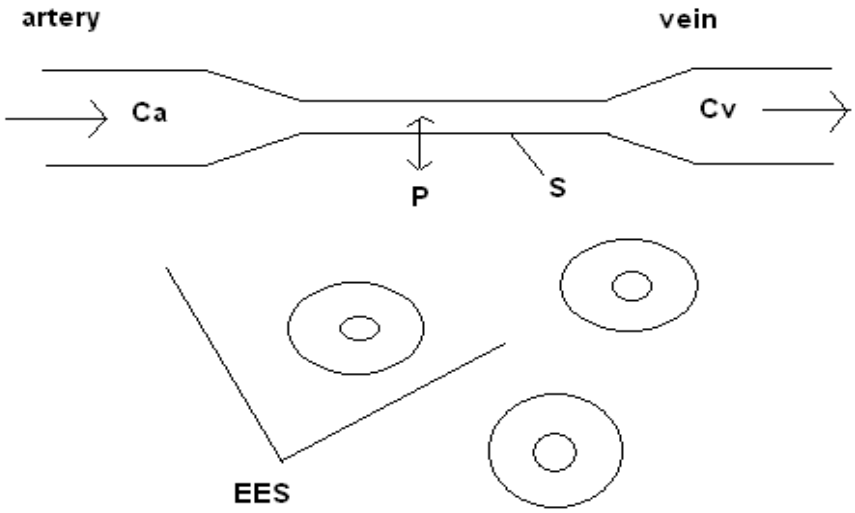

Figure 3.1 Tissue structure diagram. Blood consists of plasma (liquid part of blood) and various elements (Red blood cells, white blood cells, etc). EES (Extracellular and Extravascular Space) is an area of tissue other than the vessels and cells. Ca and Cv represent the concentration of artery and vein respectively. P means permeability and S means area.

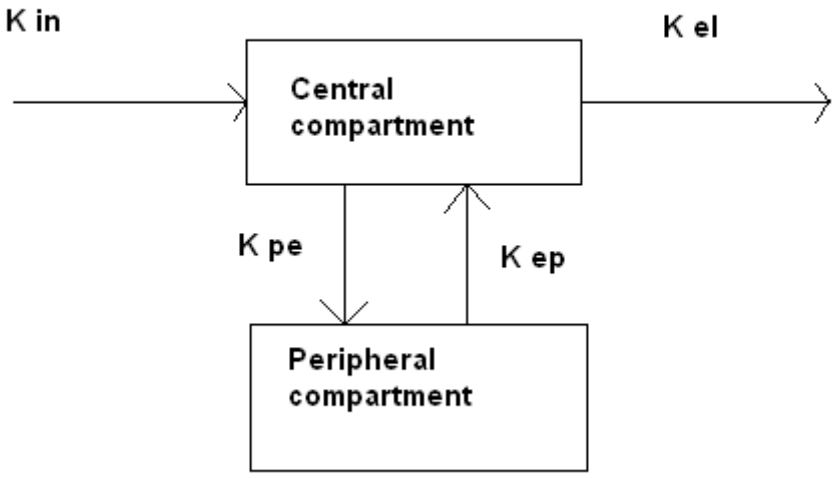

Figure 3.2 Illustration of a two compartment model demonstrating exchange of contrast agent between plasma and EES. K_{in} represents the input function from the injection of contrast agent. The central compartment refers to the plasma where the contrast is assumed to mix rapidly. The contrast exchanges with the peripheral or tumor compartment with the rate constants K_{pe} and K_{ep}. (From [21])

Table 3.1 Definitions of parameters in the differential equation describing the two compartment model.

K^{trans}	Transfer constant between blood plasma and EES	Function of permeability and flow	1/min
v_e	Volume of EES per unit volume of tissue	$v_e = \frac{V_e}{V_t}$	none
k_{ep}	Rate constant between EES and blood plasma	$k_{ep} = \frac{K^{trans}}{v_e}$	1/min

blood vessels in many solid tumors has been shown to deviate markedly from normal hierarchical branching patterns. Therefore, blood flow in a tumor is both spatially and temporally more heterogeneous than the efficient uniform perfusion of normal organs and tissues. Tumors often differ markedly from the surrounding organ in the permeability of their capillaries. This altered permeability is important in itself, because it changes the rules governing the transfer of compounds between blood and tumor tissue. Malignant tumors differ from normal tissue i) in the blood flow and volume characteristics of their microvessels, ii) in microvascular permeability, and iii) in increased fractional volume of the EES compartment. Therefore, by measuring or estimating the physiological parameters such as K^{trans}, v_e, and k_{ep}, we can get information about the tumor.

3.2.3 Time series signal of DCE MRI

DCE MRI is performed by obtaining sequential MRI images, before, during, and following the injection of a contrast agent. T_1 weighted imaging is used to observe the spread of contrast agent from the vascular space to EES, providing information about blood volume and microvascular permeability. The accumulation of contrast agent in the area of interest results in a signal increase on the T_1 weighted image. Signal intensity ($S(t)$) will change in proportion to the contrast agent concentration (C_{tumor}) in the volume element of measurement. In DCE MRI, signal intensity $S(t)$, which is obtained from the sequence of T_1 weighted images, is used to estimate the parameters in the equation derived from the pharmacokinetic model. For example, in our two compartment model case, $S(t)$ can be used to estimate K^{trans}, v_e, and k_{ep} in equation (3.1).

3.2.4 Two compartment model case

Equation (3.2) below was used to fit the time series data for each pixel where E_R, K_{el}, K_{ep} are parameters to be estimated .

$$\frac{S(C_t)}{S_0} - 1 = \frac{E_R}{K_{el} - K_{ep}} \left[e^{-K_{ep}(X - X_{tag})} - e^{-K_{el}(X - X_{tag})} \right] \qquad (3.2)$$

Equation (3.2) can be derived from equation (3.1) [22]**.** C_t is the tracer concentration in the leakage tissue, and K_{trans} is the volume transfer constant and is equal to the permeability surface area product (PS) multiplied by tissue density (ρ), $PS\rho$, $K_{ep} = K^{trans} / v_e$,where v_e is the dimensionless fraction representing the EES per unit volume of tissue. Also $E_R = T_{10} r_1 C_{p0} K^{trans}$ is the initial enhancement rate and K_{el} is related to the slope of the final part of a signal intensity curve (elimination part).

3.2.5 Model free parameter IAUGC

The IAUGC (initial area under Gd-concentration curve) method was developed to provide a robust indicator of tumor vascular characteristics. This method does not attempt to estimate directly physiological parameters related to tumor vasculature, but instead it provides a measurement of the initial arrival of contrast agent in the tissue after the contrast agent administration, which may reflect blood flow, vascular permeability and the fraction of interstitial space [23, 24]. As the linear approach was a well-approved model [23, 25], it was chosen in this study for underlying the following linear relationship between the acquired MR signal intensity and contrast agent concentration, $c(t) : S(t) = S(0) \cdot (1 + k \cdot c(t))$, where $S(t)$ and

$S(0)$ are the signal intensity of post-enhancement at any time *t* and *t=0, k* is a tissue-, sequence-, and contrast agent-dependent proportional constant. It is noted that this approach is valid only under the condition of $(TR \cdot c / T_1) << 1$. Consequently, signal linearity is limited to low contrast concentrations. In this study a trapezoidal integration of the contrast agent concentration with time over the postcontrast agent arrival was calculated in the enhancing voxels of interest:

$$IAUGC = \sum_{n=0}^{N-1} \frac{\left(c_t(n) + c_t(n-1)\right)\left(t(n) - t(n-1)\right)}{2} \qquad (3.3)$$

3.3 Methods and results

Data acquisition and analysis

Eight canine brain tumors were evaluated using a clinical 3T HDx magnet (General Electric Healthcare, Milwaukee, WI.). All tumors were confirmed histopathologically using tissue obtained from either necropsy or surgery. A paramagnetic contrast agent, Magnevist (gadopentetic acid, also known as gadopentetate dimeglumine or Gd-DTPA, by Bayer Healthcare) was injected as a bolus (0.1mMol/lb) about 5 seconds after the MR scan started. A T1-weighted fluid-attenuated inversion recovery (FLAIR) MR scan was used to acquire the DCE-MRI data. The sequence parameters were: time of repetition (TR) = 2500 msec; time of echo (TE) =5.7 msec; inversion time=700 msec; Echo train=10; bandwidth=31.25 KHz; matrix size=256 x 256 and twenty five phases separated by 8 seconds per phase for 4 cases, matrix size=512*512 and twenty five phases separated by 14 seconds per phase for the other 4 cases; field of view (FOV) =22cm; and slice thickness = 4mm. . One data set had a motion artifact during its scanning. The FSL (FMRIB Software Library, the university of Oxford) built-in

function, mcflirt, was used for motion correction. The enhancing tumor area was picked up by an edge detection algorithm from the MATLAB (The Mathworks, MA.).

Model fitting and the IAUGC were performed on a voxel-by-voxel basis within the tumor volume. For model fitting, the time series from each voxel was analyzed by using a nonlinear least square curve fitting toolbox by MATLAB. For the IAUGC, the time series of the first 90 seconds post-enhancement, recommended by the NIH, was used according to Equation (3.3).

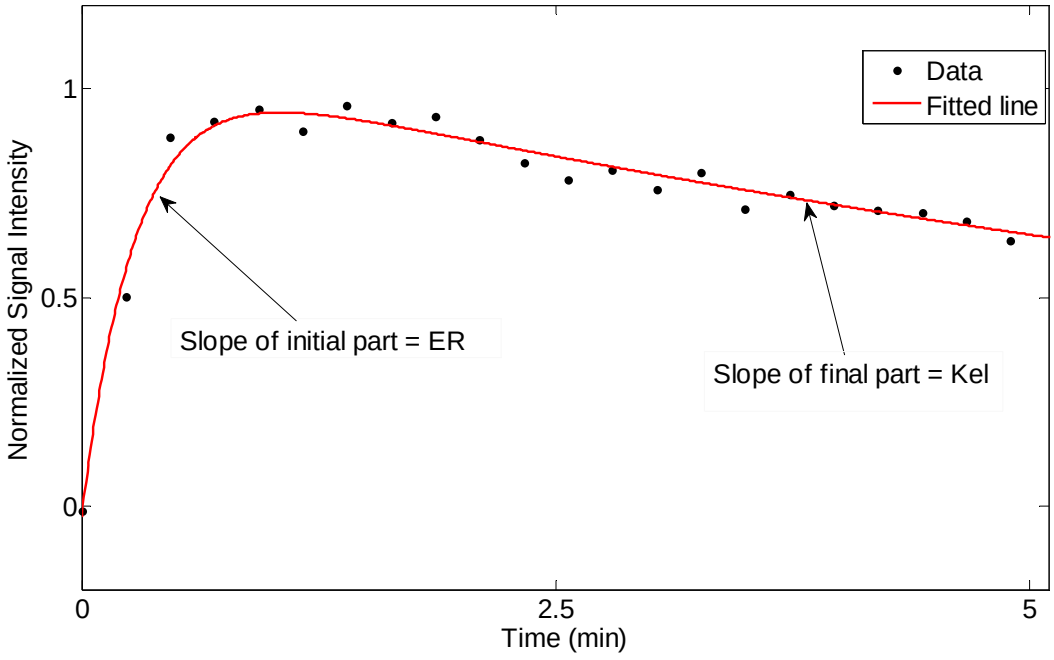

Figure 3.3 Typical time series pattern for the tumor area. Circled data points in this figure indicate the signal intensity of a voxel at a given specific time. The signal in this figure is the signal intensity at a voxel in case1 with row=250 and column=250. E_R is related to the initial enhancement rate (slope of the initial rise in the curve) and K_{el} is related to the slope of the final part of the curve (elimination part). The R-square of this non linear fitting was 0.8377..

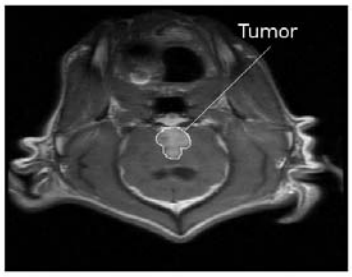

a. Denocarcinoma (date0211, case1)

b. Ependymoma (date0424, case2)

c. Meningioma (date0501, case3)

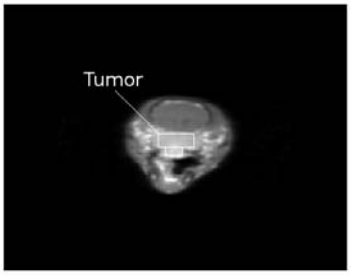

d. Carcinoma (date0603, case4)

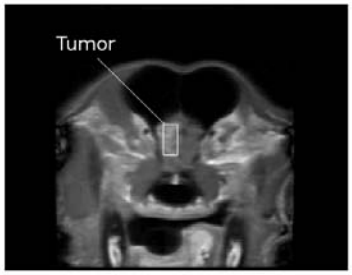

e. Meningioma (date0623, case5)

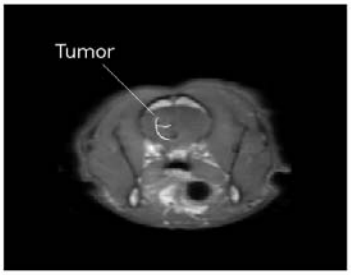

f. Oligodendroglioma (date0711, case6)

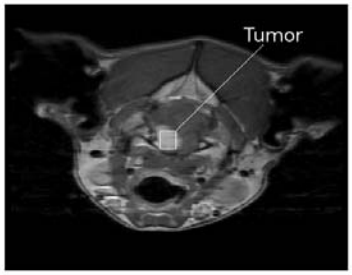

g. Meningioma (date0728, case7)

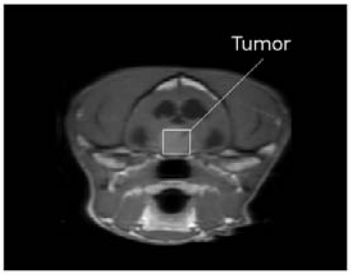

h. Macroadenoma (date0807, case8)

Figure 3.4 Illustrations of the eight canine brain tumors

A T-test was performed based on the estimated kinetic model-based parameters and model-free parameter to investigate differences between each of the two tumor types. Pearson's correlations were calculated between the three parameters, E_R (rate of enhancement, min^{-1}), K_{el} (rate of elimination, min^{-1}), K_{ep} (rate constant, min^{-1}) with the model free parameter IAUGC to find out potential correlations between the two approaches.

Results

Three physiological parameters (E_R, K_{ep}, and K_{el}) were estimated using a MATLAB nonlinear least square curve fitting toolbox for all 8 cases. Also, a trapezoidal integration of the enhancement curve (IAUGC) was calculated using equation (3.3) with time over the first 90-second (suggested by the National Cancer Institute of the National Institutes of Health). The kinetic parameters, E_R, K_{ep}, and K_{el}, and the model-free parameter, IAUGC, were presented in Table 3.2 below.

Table 3.2 Kinetic model parameter (ER,Kep, and Kel) and model-free parameter (IAUGC).

	Case#1	Case#2	Case #3	Case #4	Case #5	Case #6	Case #7	Case #8
ER (min^{-1})	2.3325 ± 0.7874	6.7442 ± 1.3862	2.6919 ± 1.2207	5.2480 ± 2.6232	2.4832 ± 0.9980	1.0169 ± 0.2775	2.8503 ± 0.2866	1.4353 ± 0.2034
K_{ep} (min^{-1})	2.5037 ± 1.0126	5.3753 ± 1.1920	3.1417 ± 1.1455	7.0551 ± 1.1954	3.3840 ± 0.9205	5.4403 ± 1.3918	2.1838 ± 0.1542	3.3257 ± 0.4372
K_{el} (min^{-1})	0.1228 ± 0.0564	0.0359 ± 0.0123	0.0330 ± 0.0201	-0.0064 ± 0.0376	-0.0285 ± 0.0436	-0.0645 ± 0.0536	0.0909 ± 0.0115	0.0586 ± 0.0610
IAUGC	50.684 ± 14.3642	88.0230 ± 16.9360	60.3950 ± 15.8999	69.0286 ± 8.6895	54.4480 ± 23.7310	19.3644 ± 6.7383	75.5099 ± 7.6015	28.7566 ± 2.0786

The eight tumors were histopathologically confirmed to be meningioma (3 cases), carcinomas (2 cases of pituitary macroadenoma, and 1 case of nasal carcinoma), ependymoma (1 case), and oligodendroglioma (1 case). Based on this histopathology result, eight tumors were categorized into 4 groups (see Table 3.3). Figure 3.5 presents histograms of the three kinetic parameters and the model-free parameter IAUGC for the four groups of tumor, respectively. The mean and standard deviations were reported in Table 3.4.

Table 3.3 Four different categories of tumor

Group	Cases	Sample size
Group1 (Meningioma)	Case3, Case5,Case7	1748
Group2 (Ependymoma)	Case6	91
Group3 (Oligodendroglioma)	Case2	1992
Group4 (Denocarcinoma, Carcinoma, Macroadenoma)	Case1,Case4,Case8	2354

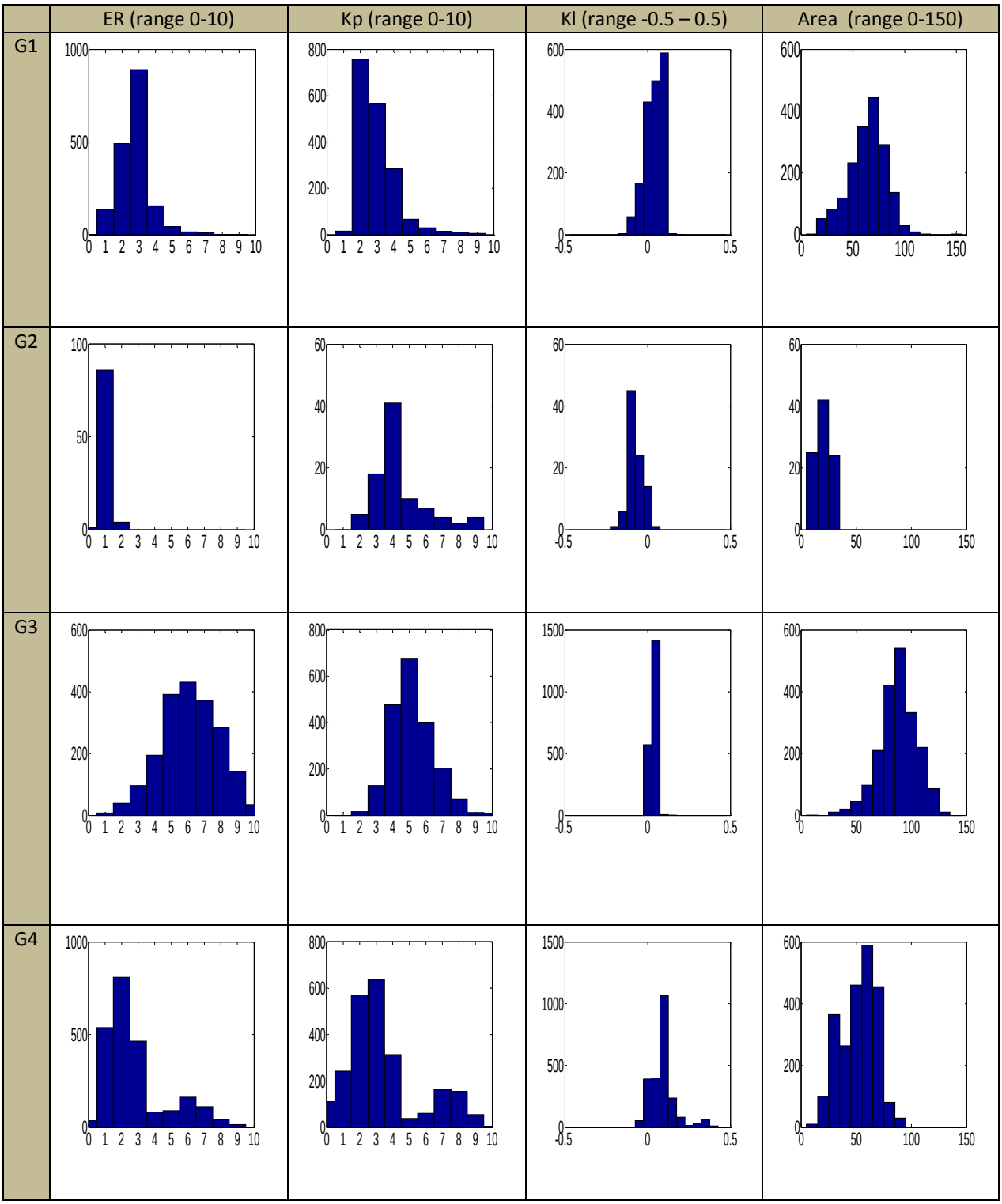

Figure 3.5 Groupwise distribution (histogram) of the three kinetic parameters (E_R, K_{ep}, and K_{el}) and model-free parameter IAUGC. The mean and standard deviation are shown below each histogram.

Table 3.4 : Group estimates (mean and standard deviation) of three kinetic parameters (E_R, K_{ep}, and K_{el}) and model-free parameter IAUGC

	E_R	K_{ep}	K_{el}	IAUGC
G1	2.7431 ± 0.9567	2.9705 ± 1.0922	0.0380 ± 0.0529	64.1442 ± 18.1060
G2	1.0083 ± 0.2680	4.4221 ± 1.5303	-0.0737 ± 0.0438	19.3644 ± 6.7383
G3	6.1166 ± 1.7295	5.1589 ± 1.2440	0.0330 ± 0.0155	88.0230 ± 16.9359
G4	2.7945 ± 1.8741	3.4165 ± 2.2214	0.0939 ± 0.0761	52.2343 ± 16.2715

First, a ANOVA (Analysis of Variance) test for each parameter was performed to test the null hypothesis that the average parameter values for 4 groups (G1,G2,G3, and G4) were equal. Since all the ANOVA tests show significant results ($P<0.001$), it was seen that at least one of the means are not equal. To find out between-group differences, group-wise differences of the kinetic parameters and IAUGC are shown in Table 3.5. A T-test was performed for each between-group difference. Except for the E_R between group one and group 4 ($P=0.253$), all other between-group numbers have significant differences with $P<0.001$.

Table 3.5 Between-group differences (mean and standard error) of three kinetic parameters (E_R, K_{ep}, and K_{el}) and the model-free parameter IAUGC. T-tests were performed and the results indicated that all, except for one (G1 vs G4 in shaded area), are significantly different with $P<0.001$.

	E_R	K_{ep}	K_{el}	IAUGC
G1 vs G2	1.7348 ± 0.0362	-1.4516 ± 0.1625	0.1117 ± 0.0047	44.7798 ± 0.8285
G1 vs G3	-3.3735 ± 0.0450	-2.1884 ± 0.0382	0.0049 ± 0.0013	-23.8787 ± 0.5757
G1 vs G4	-0.0513 ± 0.0449	-0.4460 ± 0.0527	-0.0558 ± 0.0020	11.9098 ± 0.5477
G2 vs G3	-5.1083 ± 0.0478	-0.7368 ± 0.1348	-0.1067 ± 0.0046	-68.6586 ± 0.8018
G2 vs G4	-1.7862 ± 0.0477	1.0055 ± 0.1668	-0.1676 ± 0.0048	-32.8699 ± 0.7819
G3 vs G4	3.3221 ± 0.0550	1.7423 ± 0.0536	-0.0608 ± 0.0016	35.7886 ± 0.5064

Pearson's correlations were calculated to see the relationship between three kinetic parameters (E_R, K_{ep}, and K_{el}) and the model-free parameter IAUGC (see Table 3.6). Based on this table, we can see that there is a high correlation between E_R and IAUGC. However, IAUGC didn't show significant correlation with K_{ep} and K_{el}.

Table 3.6 Pearson correlations between the three heuristic parameters, E_R, K_{ep}, K_{el}, and the model free parameter IAUGC for all eight cases.

Case #	IAUGC & E_R	IAUGC & k_{ep}	IAUGC & k_{el}
Case1	0.8105	0.3042	-0.4283
Case2	0.6787	0.1418	0.0150
Case3	0.6560	0.1541	0.4223
Case4	0.7233	0.1006	0.1116
Case5	0.9273	-0.2806	0.2841
Case6	0.6079	-0.6812	-0.1311
Case7	0.9071	-0.0384	-0.1249
Case8	0.4432	-0.0272	-0.0443

3.4 Discussion

In this study, the DCE-MRI method was used to investigate eight canine brain tumors. Three parameters E_R (rate of enhancement, min^{-1}), K_{el} (rate of elimination, min^{-1}), and K_{ep} (rate constant, min^{-1}) in equation (3.2) were estimated using the data obtained in each case's tumor area (see Figure 3.4). It should be noted that equation (3.2) only holds for low concentration of contrast agent since a linear relationship between signal enhancement and the contrast concentration is assumed during the derivation of equation (3.2) and this assumption is only valid in low contrast concentration [26-28]. As pointed out by different groups [26, 27], E_R determines the initial enhancement rate or simply the slope of the initial part of the signal-

enhancement curve, K_{el} represents the rate of elimination of the contrast agent, and K_{ep} is rate constant between the two compartments, EES and plasma.

In order to check whether there is a difference between groups, mean and standard errors of group differences for each parameter were presented in Table 3.5. T-tests were performed and the results indicated that all, except for one (G1 vs G4 in shaded area), are significantly different with $P<0.001$.

It was expected that kinetic two compartment model-based assessments of the DCE-MRI time series have an advantage over the model-free parameter IAUGC in that the kinetic model represents the true underlying physiology of the pathology concerned. However, the kinetic-model based parameters are generally thought to be more susceptible to the effects of noise and fitting errors than the simpler model-free parameter, and are often assumed to be less robust. On the other hand, the model-free parameter might be assumed to be less variable as there is no data-fitting process involved, but it cannot be used as a simple surrogate for E_R despite the more significant correlation between IAUGC and E_R. Overall, the model-free parameter IAUGC can be complementary to the kinetic model-based parameters.

As seen in Table 3.4 and Figure 3.5, variations of the estimated kinetic model-based and model-free parameters are sometimes still large, making the task of differentiation of brain tumors difficult. This was partly due to limitations of the segmentation algorithm of tumor area from background. In this study a MATLAB built-in edge detection function was used with operator's manual interference. Depending on the signal-to-noise ratio (SNR) of the DCE-MRI data and enhancement in the background, segmentation results vary from case to case. A more robust segmentation algorithm (e.g. growing region- or wavelet-based method) is needed to replace the current algorithm.

CHAPTER 4. CONCLUSION

In this thesis, the contrast enhanced MRI and dynamic contrast enhanced MRI were briefly reviewed and employed as a tool for cancer detection and differentiation research. New method referred to as phase gradient mapping was proposed as a positive contrast post processing technique to detect cells labeled with paramagnetic contrast agent.

Recently, there have been many efforts to develop a positive contrast method to overcome the drawbacks of conventional negative contrast T_2 - weighted imaging. However, the methods of white marker and IRON require manipulation of pulse sequence which is a very tedious job. The SGM was proposed as a post processing method which doesn't require pulse sequence manipulation but it has inherent uncertainty which comes from an inevitable fitting procedure associated wit it. The phase gradient mapping (PGM) technique proposed in this thesis is a post processing method which doesn't require pulse sequence manipulation and doesn't have either a fitting procedure which would introduce uncertainty. The PGM produced similar positive contrast maps as that of the SGM. The PGM is different from the SGM in that it uses phase information in image space rather than echo shift in the K-space in order to get the susceptibility gradient. The problem of current post-processing methods such as the SGM and the PGM is the difficulty of differentiation between susceptibility gradient from SPIO and that from other sources such as air/tissue interface.

DCE-MRI is another application of MRI technology effective for cancer detection. The DCE-MRI use series of MRI images instead of a single snapshot to estimate the physiological

parameters related to the tissue properties. In this thesis, the DCE-MRI data were analyzed using two methods: a two-compartment pharmacokinetic model for estimation of three enhancement parameters, E_R (rate of enhancement), K_{el} (rate of elimination), and K_{ep} (rate constant); and a model-free phenomenological parameter IAUGC (initial area under the Gd-concentration curve) defined over the first 90 seconds post-enhancement.. It is shown that the heuristic kinetic parameters, together with the model-free phenomenological parameters derived from dynamic contrast enhanced MRI, present complementary information and are appropriate to differentiate thee four types of canine brain tumors although a larger prospective study is necessary.

REFERENCE

1. Jan-Henry Seppenwoolde, et al, Passive tracking exploiting local signal conservation: The white marker phenomenon. Magnetic Resonance in Medicine, 2003, 50(4): p. 784-790.

2. Venkatesh Mani, et al, Gradient echo acquisition for superparamagnetic particles with positive contrast (GRASP): Sequence characterization in membrane and glass superparamagnetic iron oxide phantoms at 1.5T and 3T. Magnetic Resonance in Medicine, 2006, 55(1): p.126-135.

3. Wei Liu, MRI using positive-contrast techniques in detection of cells labeled with superparamagnetic iron oxide nanoparticles. NMR in Biomedicine, 2008. 21(3):p.242-250.

4. Chen, et al, Application of k-space energy spectrum analysis to susceptibility field mapping and distortion correction in gradient-echo EPI, Neuroimage, 2006, 31(2):p.609-622.

5. E.Mark Haacke, et al, Magnetic Resonance Imaging: Physical Principle and Sequence Design. 1999:Wiley-Liss.

6. Atle Bjnerud, et al, The utility of superparamantic contrast agents in MRI: theoretical consideration and applications in the cardiovascular system. NMR in Biomedicine, 2004. 17(7):p.465-477

7. Kim.Y.K, et al, Preparation of Magnetically Labeled Cells for Cell Tracking by Magnetic Resonance Imaing, Methods in Enzymology, 2004, Academic Press. P.275-299.

8. Bulte J.W.M, et al, Preparation of Magnetically Labeled Cells for Cell Tracking by Magnetic Resonance Imaging, in Methods in Enzymology. 2004, Academic Press. p. 275-299.

9. Claudia M. Hillenbrand, et al, Active device tracking and high-resolution intravascular MRI using a novel catheter-based, opposed-solenoid phased array coil. Magnetic Resonance in Medicine, 2004. 51(4): p. 668-675

10. Bogdanov A.A. Jr., et al., A new macromolecule as a contrast agent for MR angiography: preparation, properties, and animal studies. Radiology, 1993. 187(3): p. 701-706.

11. Bach-Gansmo, Abdominal MRI using a negative contrast agent. British journal of radiology, 1993. 66: p. 420-425.

12. John, F.S., The role of magnetic susceptibility in magnetic resonance imaging: MRI magnetic compatibility of the first and second kinds. Medical Physics, 1996. 23(6): p. 815-850.

13. Jigen R. Reichenbach, et al, Theory and application of static field inhomogeneity effects in gradient-echo imaging. Journal of Magnetic Resonance Imaging, 1997. 7(2): p. 266-279.

14. Hannes Dahnke, et al, Susceptibility gradient mapping (SGM): A new postprocessing method for positive contrast generation applied to superparamagnetic iron oxide particle (SPIO)-labeled cells. Magnetic Resonance in Medicine, 2008. 60(3): p. 595-603.

15. Liang, Z.-P., A Model-Based Method for Phase Unwrapping. IEEE Transactions on Medical Imaging, 1996. 15(6).

16. Aziz Hatim Poonawalla, et al, Analytical Error Propagation in Diffusion Anisotropy Calculation. Journal of Magnetic Resonance Imaging, 2004. 19: p. 489-498.

17. Vonken, E.,et al, Positive contrast visualization of nitinol devices using susceptibility gradient mapping. magn Reson Med., 2008. 60(3): p. 588-94.

18. Hylton, N., Dynamic Contrast-Enhanced Magnetic Resonance Imaging As an Imaging Biomarker. J Clin Oncol, 2006. 24(20): p. 3293-3298.

19. J P B O'Connor, et al, DCE-MRI biomarkers in the clinical evaluation of antiangiogenic and vascular disrupting agents. British journal of cancer, 2007. 96: p. 189-195.

20. Paul S. Tofts, et al, Estimating kinetic parameters from dynamic contrast-enhanced T1-weighted MRI of a diffusable tracer: Standardized quantities and symbols. Journal of Magnetic Resonance Imaging, 1999. 10(3): p. 223-232.

21. Peter L. Choyke, et al, Functional tumor imaging with dynamic contrast-enhanced magnetic resonance imaging. Journal of Magnetic Resonance Imaging, 2003. 17(5): p. 509-520.

22. Dagnachew W, et al, Quantifying dynamic contrast-enhanced MRI of the knee in children with juvenile rheumatoid arthritis using an arterial input function (AIF) extracted from popliteal artery enhancement, and the effect of the choice of the AIF on the kinetic parameters. Magnetic Resonance in Medicine, 2005. 54(3): p. 560-568.

23. Tofts, P., Modeling tracer kinetics in dynamic Gd-DTPA MR imaging. J Magn Reson Imaging, 1997. 7(1): p. 91-101.

24. Tofts, P., et al., Estimating kinetic parameters from dynamic contrast-enhanced T(1)-weighted MRI of a diffusable tracer: standardized quantities and symbols. J Magn Reson Imaging, 1999. 10(3): p. 223-32.

25. Hoffmann, U., et al., Pharmacokinetic mapping of the breast: a new method for dynamic MR mammography. Magn Reson Med., 1995. 33(4): p. 506-14.

26. Workie D, et al, Quantification of dynamic contrast enhanced MR imaging of the knee in children with juvenile rheumatoid arthritis based on pharmacokinetic modeling. Magn Reson Imaging, 2004. 22: p. 1201-1210.

27. Tofts, Modeling tracer kinetics in dynamic Gd-DTPA MR imaging. J Magn Reson Imaing 1997. 7: p. 91-101.

28. Jan-Henry Seppenwoolde, et al, Passive tracking exploiting local signal conservation: The white marker phenomenon. Magnetic Resonance in Medicine, 2003. 50(4): p. 784-790.